Heat Transfer and Consolidation Modeling of Composite Fiber Tow in Fiber Placement

By
Munki Lee

Dissertation submitted to the Faculty of the
Virginia Polytechnic Institute & State University
in Fulfillment of the Requirements for the Degree

Of
Doctor of Philosophy

In
Mechanical Engineering

Approved by

Dr. Robert H. Sturges, Chairman
Dr. Donald G. Baird
Dr. Michael P. Deisenroth
Dr. Charles F. Reinholtz
Dr. Donald J. Leo

Key Words: Heat Transfer, Composite Manufacturing, Fiber Placement, Modeling, Consolidation, Temperature Control

March 19, 2004
Blacksburg, Virginia

Heat Transfer and Consolidation Modeling of Composite Fiber Tow in Fiber Placement

By
Munki Lee

ABSTRACT

With the initial production of advanced composites, the use of composite materials has been growing rapidly in many industrial fields. The major impact has been with the weight-sensitive aerospace applications, where high strength/stiffness-to-weight ratios are very important factors. Conventionally, composites structure fabrication was conducted by hand lay-up and subsequent autoclave-based curing processes. However, the demand for cost-effective and efficient composite manufacturing is growing and thus perpetuating the replacement of existing hand lay-up processing. Automated fiber placement draws special attention for its low cost potential, flexible, and automated process. This fiber placement was investigated through the Function Block Diagram approach, and as a result, it was concluded that two sub-processes, *heat towpreg* and *compact towpreg*, are opportunity areas for better fiber placement process. This dissertation develops a heat transfer model with new heating alternatives for the *heat towpreg* sub-process and analyzes compaction force with a currently used pneumatic mechanism for the *compact towpreg* sub-process.

A linear composite towpreg was modeled with uniform material properties in one-dimension along the thickness. Thereafter, a heat transfer model between the towpreg and heating tools such as hot gas, fluid, and rigid contact heat sources, was developed. The simulation results show that a rigid contact heating is an

outstanding heating alternative from both manufacturing and energy-efficiency standpoints. The manufacturing speed of rigid contact-heating, with a constant heating temperature of 200°C is at least thirty times faster than the manufacturing speed with hot-air heating with a convective heat transfer coefficient of 260 $W/m^2/°C$. Energy efficiency of rigid heating is at least thirteen times better than the efficiency of hot air heating.

To further develop the rigid contact heating, a conceptual model of a linear two-dimensional finite element roller was employed along radial and angular directions. The roller was modeled with a transparent Pyrex tube coated with Teflon on the outer surface and a radiant heating filament coil inside. From a static-heating simulation of the roller model, the results showed an overshoot of 45.68°C and a rise time of 0.32 seconds with an ON/OFF controller. Results also revealed an overshoot of 3.31°C and a rise time of 0.42 seconds with a proportional and derivative (PD) controller. Subsequently, a quasi-static heating simulation was carried out for the same roller specifications but with a moving roller having 120 degrees of towpreg contact angle. As a result, the final temperature of the towpreg was controlled to a desired temperature within a fluctuating band of 2.51°C using the best roller specifications and a PD controller. Therefore, a rigid contact heating with a PD controller is again found to be a promising heating alternative for automated fiber placement.

In addition, a concurrent compaction process was investigated to find the possible force variations that cause variations in a consolidation process in fiber placement. Composite manufacturing processes often use a pneumatic compaction mechanism and robotic machinery, that is, a compaction system, to apply a compaction force in the consolidation process. The static force characteristics of such a pneumatic compaction mechanism were found to have non-linear behavior, hysteresis, unless the compaction mechanism was accurately controlled. Even though a pre-regulator and a relief valve controlled the incoming air of the cylinder, the maximum hysteresis was measured as 2.04 lbs for 0.3 inches of air-cylinder compression with an inside air-pressure of 20 psi. Furthermore, dynamic steady and unsteady compaction forces were experimentally measured and analyzed through the Fast Fourier Transformation (FFT) technique. To reduce the fluctuating compaction force and to compensate hysteresis-induced variations while the compaction system runs, a spring was combined with an existing air-cylinder. Using the combined component, the compaction system achieved both a stable steady compaction force and a reduced unsteady fluctuating force. However, some fluctuation in the unsteady force is inevitable when using a robot on a worktable under a compacting load. It is concluded that the robot is the main contributor to this fluctuation.

Two major opportunity areas were investigated for the automated fiber placement process. For a towpreg heating process, heat transfer model was developed with a thin one-dimensional towpreg and conventional/alternative heat sources to estimated manufacturing speed and energy efficiency. Subsequently, the best heat source with the towpreg was modeled to gauge the controllability of a heating temperature. Furthermore, a compaction force with the pneumatic compaction mechanism was analyzed in detail for its possible effect on the composite quality for a towpreg consolidation process. These models, heat transfer and compaction, were discussed qualitatively and quantitatively for the fiber placement in this dissertation.

Acknowledgements

Most of all, I want to thank God All Mighty in the heaven. His mercy and love saved me and enabled me to run toward the goal of my life. Also, I want to show great thanks to my advisor, Dr. Bob Sturges, for his advising and supporting throughout the long journey of my graduate study. His passionate attitude for research will be a good exemplar of my engineering life in the future. Great thanks extend to my committee members, Dr. Donald Baird, Dr. Michael Diesenroth, Dr. Charles Reinholtz, Dr. Donald Leo, and Dr. Dennis Hong for their kind advising and significant contributions to my research work. My office mates, Junghun, Mike, Roger, have been good friends of mine during my school years in Virginia Tech.

Endless love of my wife, Yoojin Jo, made me successfully finish my study in Virginia Tech. The everlasting love of hers and my two sons' always has been encouraging energy of mine. Special gratitude must be expressed to my parents, Wooyeol Lee and Junghee Lee, and parents in law, Soohyun Jo and Haesoon Sul, my brother and sister. Without their loving supports, I am sure that I could not have finished. Beautiful life in Blacksburg with good neighborhood will go forever throughout my life.

To my loving family
Andrew Jeeyoon, John Jeemin, Yoojin

Table of Contents

List of Figures

List of Tables

1 Introduction

1.1 Problem Statement

Composites, which are homogeneous materials created by at least two materials, were developed to reach a much higher strength and stiffness, and, at the same time, achieve a much lighter weight than the original materials. The characteristics of the materials have had an impact on many commercial manufacturing fields, especially on weight-sensitive aerospace applications. However, the high manufacturing costs of hand lay-up have been a big handicap for rapidly growing applications of the composites. Automated fiber placement, as one of the composite manufacturing techniques, has gained attention for its cost-effective, flexible, and automatic process [21~23,32,40,41].

The automated fiber placement process is a mixture of physical and chemical phenomena, such as heat transfer from heating tools to an incoming composite towpreg, a compaction process to compress the heated towpreg to a substrate, and a subsequent bonding of the two materials. Each sub-process is sequentially accomplished by computer-controlled robotic machinery [46,47]. Investigation of the process through the Function Block Diagramming (FBD) approach shows that heating towpreg and compressing towpreg have opportunities to be improved by a deeper understanding and further analyses of the sub-processes.

First, heat transfer between the heating system and an incoming towpreg is not easily controllable with current heat sources and, accordingly, results in much energy loss and non-consistent towpreg heating. Hence, new heating alternatives, liquid and a rigid contact, are suggested and compared with a widely used gas-heating source. Energy efficiency and finalized-parts quality are foremost considerations in the automated fiber placement process.

Second, the consolidation process that places the heated towpreg on a substrate needs to be investigated. Most industries in automated composite manufacturing fields rely on computerized robotic technologies with a pneumatic compaction mechanism. However, little research has been done that shows a compaction mechanism and robotic machinery in a composite fabrication process have their own tolerances, positional/speed errors, and possible variations. The integrated tolerances and possible variations of the compaction system under an external load condition, may result in a non-consistent compaction force during the automated fiber placement as shown in Figure 1. Hence, a clearer understanding of the compaction process is needed; specifically, controllable parameters of the physical compaction should be found.

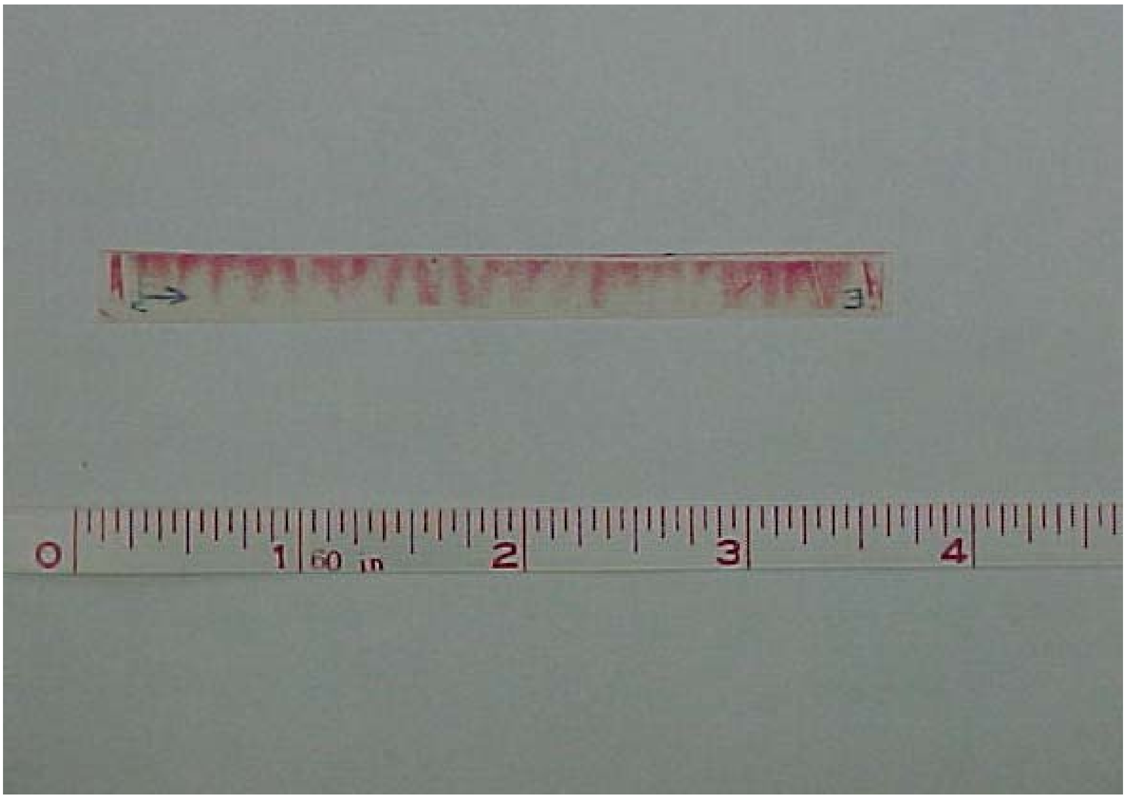

Figure 1. Compaction Force Profile with a Roller End-effector on the Tactile Force/Pressure sensor

1.2 Objectives

New heating techniques are required to better control heat transfer between heating tools and a composite towpreg in the automated fiber placement process. This dissertation suggests new heating techniques with liquid and rigid contact heat sources, and compares them with a widely used gas heat source for the fiber placement process.

A thin towpreg composite model needs to be developed to describe the heat transfer. Subsequently, the response of the towpreg with each heat source will be compared from manufacturing speed and energy efficiency viewpoints. The most promising heat source will be developed for heat transfer modeling between a moving towpreg and dynamic heat source in the automated fiber placement. Through the heat transfer model, both the temperature controllability of the towpreg and manufacturing speed could be investigated.

In addition, an accurate compaction process is needed in response to the growing demand for better composite processing. Since the errors in compaction mechanisms and robotic machinery in fiber placement have not been discussed in the literature, experimental investigation to address possible reasons for the variations in the compaction force needs to be conducted with a compaction mechanism. A clearer understanding of the physical compaction process can lead to controllable process parameters for consistent ply compaction, such that the final parts quality can be enhanced.

Even though this dissertation investigates the thermoset fiber placement process, the proposed approach could be universally applicable to other composite-fabrication processes. It is hoped that the modeling and analysis could substantially contribute to composite manufacturing fields.

1.3 Automated Fiber Placement

Historically, advanced composites have been manufactured by hand lay-up of prepreg to produce composite parts that are then consolidated and cured in an autoclave. This manual process results in high fiber volume fraction, void-free, well-consolidated composite structures with excellent mechanical properties. However, the costs of these structures are high due to the labor costs for hand lay-up processing [1].

Automated fiber placement is currently a more accepted technology in composite manufacturing fields, because the process can achieve design flexibility, cost-effectiveness, and in-process compaction. This process shown in Figure 2 consists of towpreg supplying, laying the towpreg on a substrate, in-situ compaction, and cut-clamp and restart of the towpreg sequentially. By automating each of these steps, hand lay-up could be eliminated. Additionally, fiber placement that is a logical combination of filament winding and automated tape placement offers novel characteristics to overcome some of the limitations of each manufacturing method [40,47]. The fiber placement process uses multiple narrow towpregs, such that the fiber buckling associated with tape placement on a complex shape is eliminated. Also, the fiber placement has features that are not available with filament winding: precise control of fiber angles, debulking of material on the fly, and cutting alternatives for many applications [47]. The manufacturing advantages and disadvantages of the fiber placement process and other processes are compared in Table 1.

Table 1. Thermoset Manufacturing Method Comparison [40,47]

Fiber Placement	**Filament Winding**	**Tape Laying**	**Hand Lay-up**
Geodesic and Non-geodesic	Geodesic Path only	Geodesic Path only	Geodesic and Non-geodesic
Convex and Concave	Convex Surface	Convex and Concave	Convex and Concave
Start and Stop Fibers	Endless Fibers	Start and Stop Fibers	Start and Stop Fibers
In-process Compaction	In-process Compaction	In-process Compaction	Compaction in Autoclave
Constant Ply Thickness	Non-constant Ply Thickness	Non-constant Ply Thickness	Constant Ply Thickness
Accurate and Repeatable	Accurate and Repeatable	Accurate and Repeatable	Not Accurate and Non-Repeatable
Lap/Gap Controllable	Lap/Gap Controllable	Lap/Gap Controllable	Lap/Gap Non-controllable
Reduced Labor Cost	Reduced Labor Cost	Reduced Labor Cost	High Labor Cost
Flexible Design	Non-flexible Design	Non-flexible Design	Flexible Design

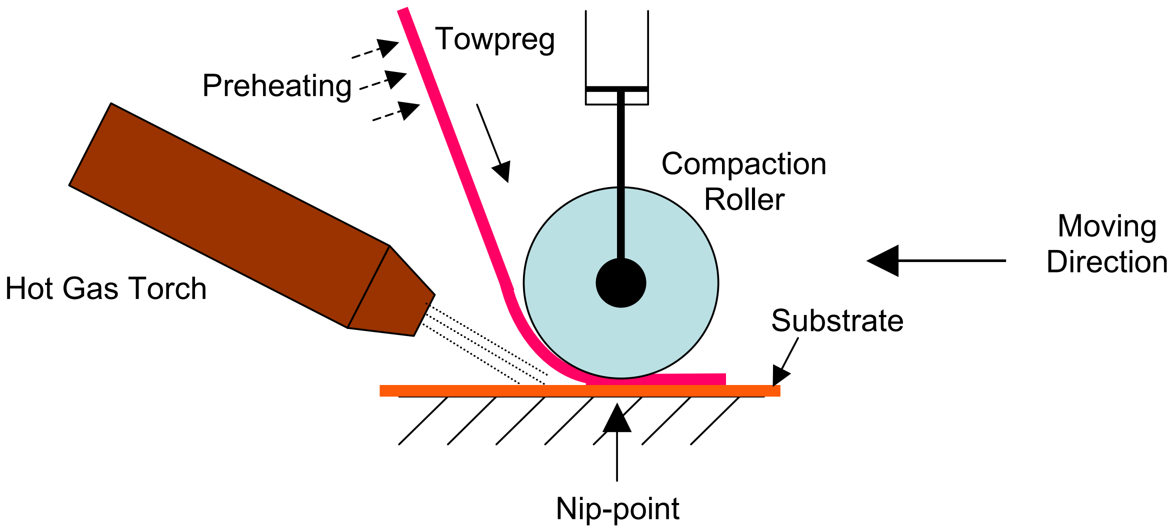

Figure 2. Schematic Diagram of Automated Fiber Placement Process

1.4 Function Block Diagramming Approach

The Function Block Diagram (FBD) approach for conceptual design has been used for several decades to provide a common language for specialists in multiple domains. Its systematic approach routinely provides better understanding and process information identification. The Function Block Diagram approach [4] expresses the main objective at the far left side and terminates with specific component information at the far right side in the diagram. The function block or node in the diagram contains the function name (what is done) expressed as a generic noun/verb pair to describe the function of the product or process [5,6], and the overall structure reveals the how/why relationships between them. The left, higher-level, function blocks of each function represent "why" the function is included. In addition, the right blocks, which are lower-level blocks, represent "how" the function is performed. The issue in this conceptual design theory is to understand the processes that lead to innovation and create tools which generate such step changes in function and that in an orderly basis. One of the important contributions of this approach is its ability to capture design intent through a chain of reasoning and to highlight the dependencies among the sub-functions of a design.

1.4.1 Developing Function Block Diagram (FBD) for the Automated Fiber Placement Process

For the advanced composite fiber placement process, the main objective is "Fabricate composite." This logically decomposes into many specific functions and artifacts as shown at the far right of Figure 3. Dotted function blocks in this

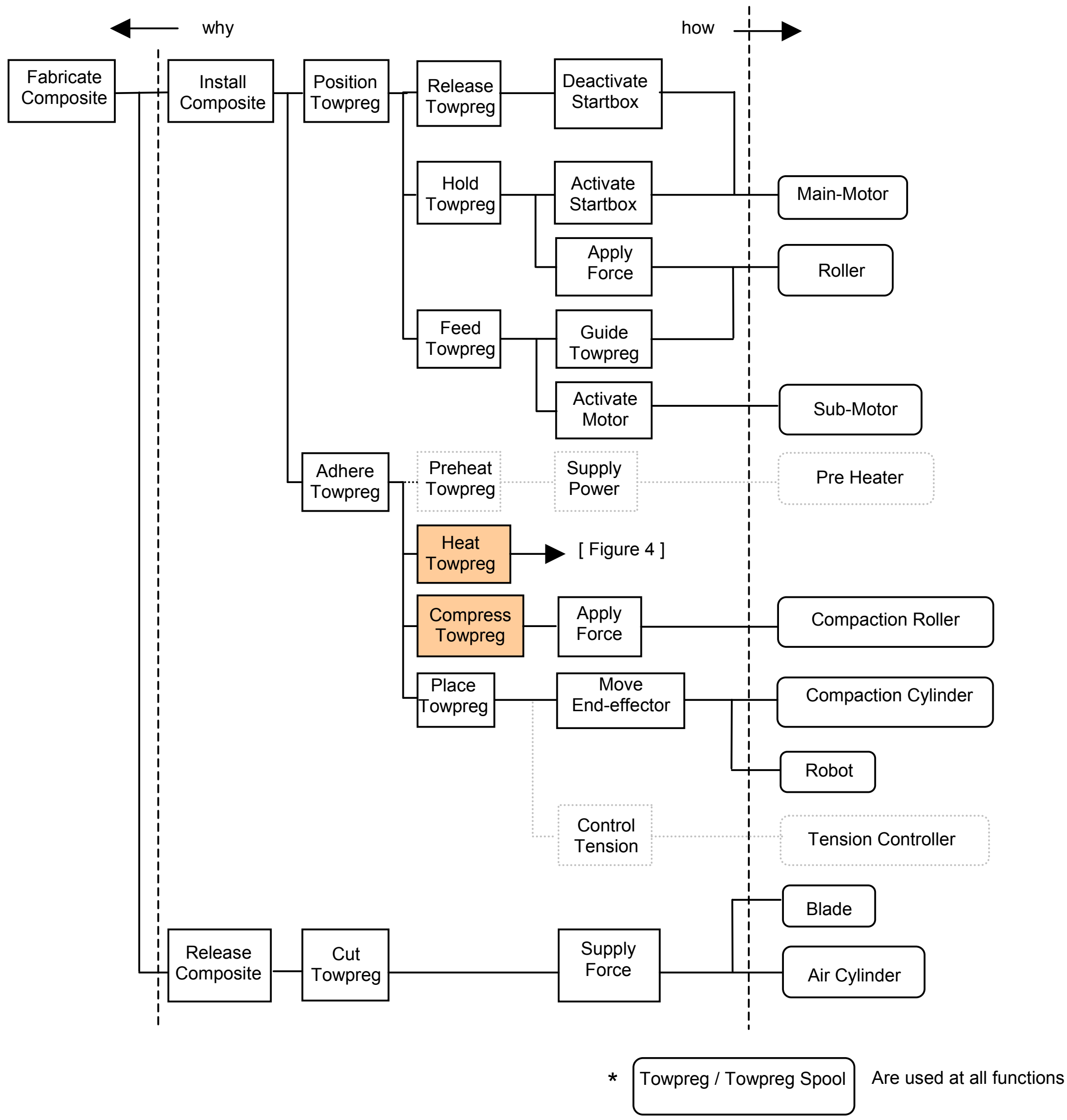

Figure 3. Function Block Diagram for Composite Fiber Placement Process

figure refer to alternatives according to the specific manufacturing environment. It was found that *heating towpreg* and *compress towpreg* functions are opportunity areas for efficient and accurate manufacturing processes. Hence, the heat source for *heating towpreg* function block and compaction mechanism for *compress towpreg* were investigated in detail.

The major parameters of the advanced fiber placement process are preheating temperature, nip-point temperature, compaction force, towpreg tension, manufacturing speed, and diffusivity of a composite [26,39,40,45,54]. Some process parameters, such as manufacturing speed and towpreg tension, can be easily controlled using fiber placement machine controllers. However, the heat transfer from a heat source moving over a substrate is a major factor in the final part quality and is difficult to control [17]. The control cost of a complex controller with sensors to achieve good heat transfer is very high, such that the main cost issue of composite fabrication arises again. Thus, an alternative heating concept for efficient towpreg heating is strongly required to better control the heat transfer from a heating tool to a composite towpreg. For this requirement, conceptual sub-function block diagrams with alternative heat sources are developed.

1.4.2 Sub-Function Block Diagram with Alternative Heat Sources

Heat sources, such as laser, infrared, and hot gas torches, have been used currently and widely for automated composite fiber placement. A hot gas torch is most frequently used for its installation flexibility and low cost. In addition to these current and widely used heat sources, two more new heat sources, liquid and rigid contact, are conceptualized in Figure 4 ~ Figure 6. According to the heat source selected, corresponding major parameters and specific components change. For a gas heat source, major parameters are the temperature of the hot gas torch, gas flow rate, distance between the torch and composite, and manufacturing speed associated with composite tension as in Figure 4. For a liquid heat source, major parameters are similar to those of a gas heat source, except for the effect of the liquid's thermal properties and re-circulation of the liquid as shown in Figure 5. On the other hand, the main parameters of a rigid heat source are the thermal properties of a rigid roller and a non-stick contact surface as indicated in Figure 6. From this analysis, we identify the following focus areas for study: heat transfer modeling of a towpreg with different heat sources, modeling of the most promising heat source in contact with the towpreg, and compaction force analysis, which will be discussed in the next chapters.

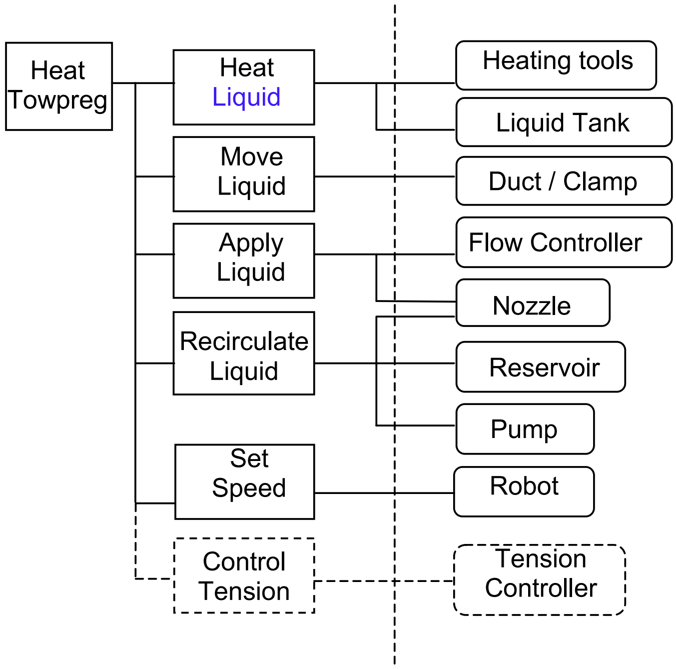

Figure 4. Sub-Function Block Diagram for Heating Composite Towpreg with a Gas Heat Source

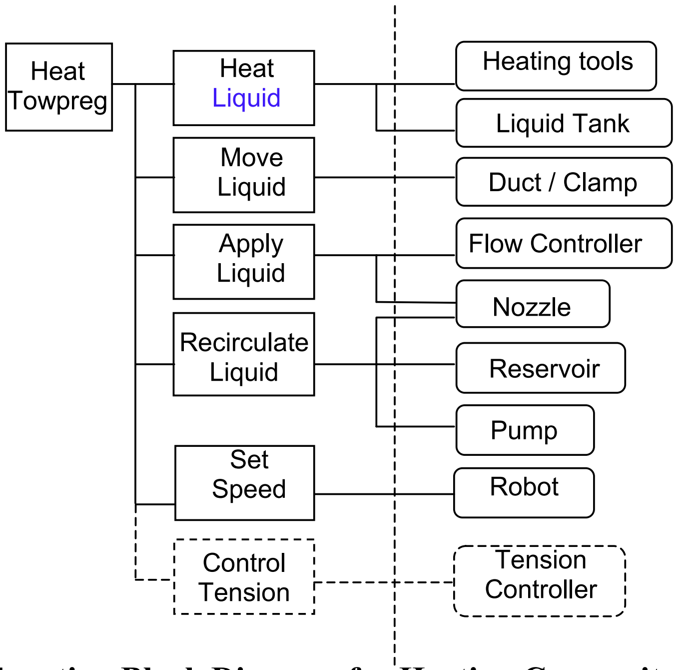

Figure 5. Sub-Function Block Diagram for Heating Composite Towpreg with a Liquid Heat Source

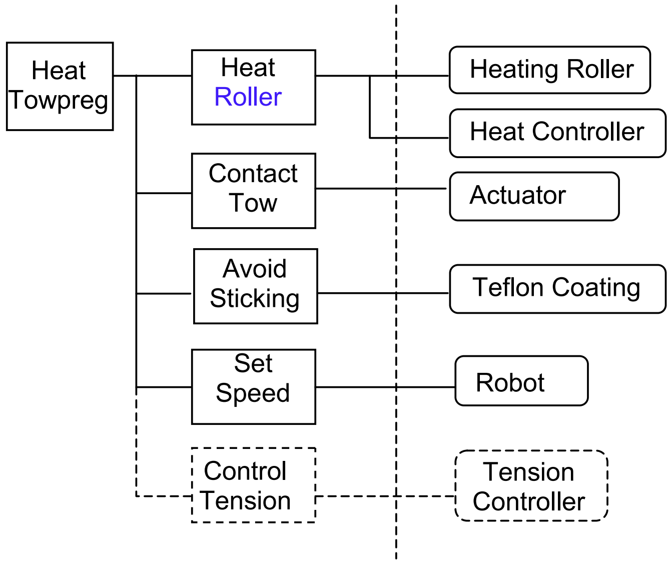

Figure 6. Sub-Function Block Diagram for Heating Composite Towpreg with a Rigid Contact Heat Source

1.5 Heating Alternatives for Fiber Placement

In order to allow high-speed production at high temperature, a powerful heating source has to be incorporated. Furthermore, the response time of the heaters needs to be as quick as possible with a stable performance. Weight, size, flexibility, and price are also important considerations for heating tool selection. Three currently and widely used heating tools for flexible composite manufacturing are compared qualitatively in Table 2.

Table 2. Qualitative Comparison of Three Heat Sources [40]

	Hot Gas Torch	Laser Beam	Infrared Light
Energy Efficiency	– –	+	+/–
Response Time	–	+	+/–
Size	+ +	–	+/–
Weight	+ +	–	+
Price	+/–	–	+

Note: + : Good , + + : Very good , – : Bad , – –: Very bad

Laser beam heating is an excellent heating technique for energy-efficiency and fast response time. However, it has size and weight limitation problems. Infrared light heating is, overall, a good technique, because of its energy-efficiency and small size with a reasonable price. The hot gas heating method is the most widely used for its cost-effectiveness and design-flexibility even though it has the disadvantages of very low energy efficiency and slow response time. In many composite manufacturing processes, combined heating, for example, preheating with an infrared light and major heating with hot gas torches, is used to reduce void content in finalized composite parts [26] and to reduce the risk of overheating at the nip point. The heat sources have been well discussed from a variety of viewpoints for thermoset/thermoplastic fiber placement or thermoplastic filament winding [17~37,39~41].

Alternative heat sources, liquid and a rigid contact, have yet to be studied for the composite manufacturing process. To quantitatively investigate these two heating alternatives, the most widely used heating tool, a hot gas torch, is compared from the manufacturing-speed and energy-efficiency viewpoints. The liquid heat source has a higher forced-convective heat transfer coefficient than the coefficient of a hot gas heat source. The coefficient is an important factor in convective heat transfer between a heating tool and a composite towpreg. The rigid contact heat source uses conductive heat transfer to apply heat to the composite towpreg. The conductive heating, of course, is a much more energy-efficient and faster heating method than convective heating. This dissertation answers two questions: first, “How much faster and energy-efficient are the heating alternatives than gas heating?” and, second, “What are advantages and disadvantages for different heat sources?.”

1.5.1 Heat Transfer Modeling of a Composite Towpreg

To compare these three heat sources, namely, hot gas, liquid, and rigid contact, a one dimensional thin towpreg model is employed to describe heat transfer between the towpreg and each heat source. It is known that composite material has non-linear governing equations and non-linear material behaviors [1,3,7]. However, to quantify the response time and energy efficiency for the three heat sources, linear equations with uniform material properties are used to solve the heat transfer equations from each heat source to the towpreg. Since the target composite towpreg is very thin, the possibilities of nonlinear governing equations and non-uniformity along the thickness could be neglected.

First, for the same effective heating area with the three heat sources, static towpreg modeling is developed to gauge the response time and thus to identify important parameters that significantly affect this response. Effective composite length divided by the response time for each heat source is equal to the manufacturing speed of the towpreg with the heat source. Second, energy efficiencies for the three heat sources are compared with the same composite towpreg model, but in this case with a linearly moving model through the same effective heating area. Since manufacturing speeds can be calculated using the static towpreg model for the three heat sources, energy efficiencies can be calculated while the towpreg moves through the effective heating area with the manufacturing speeds.

Simulation results show that the rigid heating is an outstanding heating alternative in both manufacturing speed and energy-efficiency. Hence, how to realize the rigid contact heating potential and by what processes it could be quantitatively improved are discussed in the following sections.

1.5.2 Modeling of a Rigid Heating Roller in Contact with a Composite Towpreg

A rigid-contact heating roller using internal radiation is widely used for fusing and bonding toner to paper in a xerographic machine or a printer. Model of the roller was developed for fusion roller temperature control [17,18]. In the model, however, the paper contact area of a rigid contacting roller is small, and heat transfer to the paper is very little. In comparison, a rigid heating roller in composite manufacturing application needs a large towpreg contact area and, thus, significant amount of heat transfer between the two materials should be considered.

To further develop the rigid contact-heating technique in composite fiber placement, a rigid heating roller with a hollow shape is conceptually designed to run the simulation of the heat transfer between the heating roller and the incoming towpreg. The roller is made of a hollow transparent Pyrex material with a Teflon coating outside and with a heating filament coil inside. To quantify heat interactions of the roller and the thin composite towpreg, uniform material properties and linear heat transfer equations are used with no external disturbance. A Finite Element Method (FEM) in a Matlab PDE Toolbox is employed to simulate both a static rigid roller and a dynamic rigid roller, because the discrete and approximate approach can easily solve a mathematical heat transfer model both with and without varying boundary conditions.

Statically, the temperature-rising profile of the stationary heating roller was investigated with either an ON/OFF or a PD controller. Physical responses, a rise time and an overshoot, of the roller surface were estimated without contacting a towpreg. For quasi-static heating, temperature variations of the heating roller and the towpreg are described where the roller is in contact with the towpreg. Since the roller has a rolling contact with the towpreg, the linear speed of the roller is the same as the towpreg feeding speed, meaning that it is equal to the composite manufacturing speed. In addition, the consistency of the temperatures at the heating tool and the towpreg is an essential factor for the finalized composite parts quality [17,40]. Therefore, temperature controllability of the composite and the manufacturing speed are quantitatively discussed with an ON/OFF controller or a PD controller in this research.

1.6 Compaction Force Analysis

A pneumatic compaction system has been used to apply a compaction force in most composite manufacturing methods. In response to the demand for high quality of composite structures, the compaction force for a consolidation process needs to be reinvestigated for possible variations of the force that lead to the variations of the consolidation process. Ideally, the pneumatic mechanism and robotic machinery would give constant compaction force for external disturbances. Arbitrary surface shape of a structure, start/end tape-laying, and machine vibrations are the main reasons for the external disturbances. However, if a pneumatic compaction system, which comprises a pneumatic cylinder, a robotic end-effector, a robot itself, is not accurately controlled, the compaction process with this system might have undesirable non-linear behavior. Even though the compaction force is known as one of the main process parameters in the fiber placement, the possible variation of the compaction force due to a pneumatic mechanism and a robot with an end-effector has not yet been discussed.

To measure the compaction force, Merlin robot 6200 [59,60] was used with a Force/Torque sensor, JR-3 [55,56], attached to the robotic endplate. Incoming air into the air-cylinder was pre-regulated by a Wilkerson air-pressure regulator and controlled by a relief valve installed at the inlet of the cylinder. As shown in Figure 1, when a compaction roller operated by a pneumatic compaction mechanism was moved on the tactile force/pressure sensor [55] by the robot, the color of the track, which indicates the compaction force, was not uniform. Non-uniform compaction force during all kinds of composite processing techniques may result in unacceptable product variations. Hence, compaction force was studied from static and dynamic viewpoints.

The static characteristic of a pneumatic compaction mechanism with the external pressure regulator was found to have a non-linear behavior, hysteresis. The dynamic steady and unsteady compaction force profiles were analyzed to understand the physics of non-consistent compaction force during the compaction process. To achieve both a stable steady response and a reduction of a dynamically fluctuating compaction force, a spring type compaction component was combined to an existing pneumatic cylinder. The dynamic and steady quantities of settling time and overshoot were measured and compared for different compaction components. Furthermore, the dynamic and unsteady compaction force was measured while the compaction mechanism driven by the robot was moving on the worktable. The fluctuation quantity of the force was potentially significant [54], and thus needed to be reduced. Through the Fast Fourier Transformation (FFT) analysis associated with a low-pass filter, the main cause of the dynamic and unsteady compaction force was investigated.

2 Literature Review

Composite materials are the result of embedding high-strength, high-stiffness fibers on one material in a surrounding matrix of another material. The fibers of interests for composites are generally of either single fibers or multiple fibers in the form of yarn or tow. Advanced composites especially indicate those with high-performance characteristics, generally strength and stiffness, from the simpler forms as reinforced plastics [3]. The advanced composites are ideal materials for aerospace applications, where the use of high performance advanced composites directly enhances the capability of fuel-efficient aircraft and the development of new generation aerospace vehicles. The structures made of advanced composites for aerospace applications have been manufactured by hand lay-up of prepreg tape to produce composite parts that are finalized by a consolidation and a curing process in an autoclave. However, widespread use of composite materials for aerospace applications has been limited due to high manufacturing costs, long processing time and size limitation in an autoclave [1,2]. For higher performance composite structures, automated fiber placement is a promising process to achieve both desired quality and lower costs.

To investigate the automated fiber placement process, Function Block Diagramming (FBD) [4] approach is employed to identify detailed information inside the process. Sturges et al. [5,6] proposed that the logical expansion of sub-functions from “why” to “how” helps not only understanding many processes substantially but finding new design intent through a chain reasoning of the sub-functions. Through the FBD approach, two major sub-functions, *heat towpreg* and *compress towpreg*, draw attention for their potential to improve the quality of the composite. For better heating and compressing methods, new heating alternatives and detailed analysis of the compaction process are suggested respectively.

2.1 Heat Transfer Modeling

Colton and Leach [7] studied a transient one-dimensional heat transfer to find the effects of the thermoplastic filament winding process, and concluded that the winding speed was the most important parameter for the process. A numerical Finite Difference Method (FDM) was used to predict the temperature profiles of the part and tools. They discussed heating methods for localized melting of a composite using radiant heating and convective hot air heating. However, conductive heating was not considered because of its sticking problems associated with contact device. Since the time it was proposed, Sun and et al. [14] succeeded a thermoplastic composite tape-laying process using a sliding rigid contact heat for modeling and controlling the process.

Pitchumani et al. [16] presented a theoretical one-dimensional model for the thermoplastic tow placement process using torches. The model was developed to describe the heat transfer and consolidation phenomena of the process. The thermal model consists of numerically solving the energy equation subject to two principal simplifications: (a) conduction of heat in the through-the-thickness direction is dominant over conduction in the span-wise and widthwise directions, and (b) heat transfer due to the polymer crystallization process is assumed negligibly small. The bottom surface has a convective boundary condition with a large convective heat transfer coefficient, such that the bottom surface temperature is equal to the mandrel temperature throughout the process.

Bryant et al. [12] developed a direct fabrication model of curved panels made from composites. The model is based on one-dimensional transient heat conduction from a flexible heater pad to a ceramic matrix composite for the Curved-layer Laminated Object Manufacturing (LOM) process. Even though the boundary condition is a direct conduction from laminator to the composite, the mathematical model used convective boundary conditions with a convective heat transfer coefficient and a constant laminator temperature. For a constant laminator temperature (T_{lam}), a convective heat transfer coefficient (h_{lam}) was estimated through experimentally measured data. For example, with a constant laminator temperature (T_{lam}) of 110°C, the convective heat transfer coefficient (h_{lam}) was estimated as a 275 W/m^2/K.

Multi-dimensional composite models were developed for an analysis of the heat transfer during the thick tape laying process. Grove [8] developed a two-dimensional finite element model to investigate the temperature profile of the tape laying process with a single laser heat source, and Beyeler and Güçeri [9] used a two-dimensional finite difference technique to investigate an anisotropic heat conduction phenomena of the laser-assisted tape laying process. Ghasemi Nejhad et al. [19] used a two-dimensional and steady-state approach, which is similar to those proposed by Beyeler and Güçeri [9], but accounted for the size effect on the heating area for the process. They found that as the size of the heating area decreased, the processing window narrowed. The identical finite difference approach for the parametric study was later extended to include a three-dimensional thermal analysis of thermoplastic filament winding [10].

Each heat transfer model associated with a composite and heating tools in the literature has its own process and particular application, and thus, heat transfer models and corresponding process parameters change for different composite materials, specifications, and heating tools. Hence, we develop a one-dimensional heat transfer model for thin thickness composite with uniform material properties in this research to quantify the responses and to find parameters during the heating process for different heat sources.

2.2 Towpreg Heating Techniques

Conventionally, three major heating techniques, -- laser heating, infrared heating, hot gas heating -- are widely used for flexible composite fiber placement. The choice of each heating apparatus is unique and depends largely on its applications. The following section reviews various heating tool developments and their current applications.

2.2.1 Laser Heating

Beyeler and Güçeri [27] first introduced Laser heating and extended [28,29]. The CO_2 laser beam melted an incoming composite tape and substrate for thermoplastic filament winding. The towpregs were placed onto a vertical mandrel by a horizontal rotating table with an air-cylinder and a linear bearing, and later, motion controller was used make helical springs with APC-2 prepreg tows [30]. Mazumdar and Hoa [31] also used CO_2 laser for placing the APC-2 prepregs onto a steel mandrel. After the impact of processing parameters on consolidated rings was investigated and the results from double cantilever beam tests were obtained, the laser was shown to be one promising heat source for composite manufacturing. The two major advantages of the laser power were excellent energy efficiency and fast response [40]. These make it ideal to integrate the laser into a feedback control loop. For mass production parts, McDonnell Douglas Aerospace (MDA) developed a laser-assisted fiber placement machine [32]. However, the size and weight of a laser requires a large fiber placement head in order to carry it. This restriction limits the application of laser to large machines only.

2.2.2 Infrared Heating

Werdermann et al. [33] combined an infrared heating and a hot gas heating for a thermoplastic manufacturing application. For the energy-efficient characteristics with good response behavior, Endres [35] and Calhoun [36] investigated its applicability for filament winding of thermoplastic composite tapes. Although this infrared heating is not as good as laser heating, it is, overall, a good technique shown in Table 2, and a small and lightweight product with reasonable price is available on the market. However, it is not a viable solution for nip-point heating which needs very high intensity heating on the nip-point.

2.2.3 Hot Gas Heating

Werdermann et al. [33] first started to use a hot gas heating for on-line consolidation of thermoplastic composites. The hot gas heater was combined with an infrared radiation oven for nip-point heating and preheating, respectively. Buijs and Nederveen [63] extended the basic set-up of the hybrid heating system. Two pairs of an infrared pre-heater and a hot gas torch were used to promote a towpreg melting sub-process. This hybrid system was evolved one more step to a system, which had an infrared line heater right on top of the mandrel and two hot air heaters to provide constant nip-point temperature and to increase consolidation speed [34].

The hot gas heating has been mounted in a robotic or a filament winding machine for composite manufacturing. Automated Dynamic Corporation [22] developed a robotic winding system (ROWS) to place towpreg onto a stationary mandrel. Steiner [37] integrated a compact consolidation head with a 6-axis PUMA 762 robot for a filament winding process, and this robotic winding system was modified by Hummler et al. [20] to accomplish double-concave filament winding. Felderhoff and Steiner [40] again used the hybrid system mounted onto a PUMA robot for a fiber placement process.

A current hot gas torch is capable of heating the nitrogen up to 1200°C, such that fast processing on a complex-shaped surface is possible. In spite of the disadvantages of very low energy efficiency and slow response time, a hot gas heating method is the most widely used for its cost-effectiveness and design-flexibility.

2.2.4 New Heating Methods

The hot gas heating method uses a forced convective heating with a high convective heat transfer coefficient and a high gas temperature. A similar convective heating with a higher heat transfer coefficient and a lower source temperature converges to a fluid contact heating. The forced convective heating with a liquid contact, in general, has at least twice as high a heat transfer coefficient as the coefficient of a forced convective gas heating. This heating technique should be environmentally non-toxic, easily cleanable, and easily re-circulated for energy efficiency. Considering these advantages, a fluid contact heating will be investigated to compare the manufacturing speed and energy efficiency with a current gas heating.

In addition, rigid contact heating is employed for towpreg heating. An exemplar rigid contact heat source utilizing internal radiation is widely used for the fusing process in a xerographic machine or a printer. The fusing process is basically the same for all such machines. A fuser unit, which is composed of an upper metal roller and a lower soft roller, presses a paper to fuse it, and thus permanently bonds the toner to the paper by means of heat and roller pressure. In case of a printer, the upper roller has a hollow-shape is heated with a temperature-controlled Tungsten-Hallogen lamp and covered by a non-stick/easily cleanable Silicon Teflon coating [38]. The lower roller is coated with a soft blanket of red silicon rubber and generally is not heated.

Since the conventional fusing roller has a low thermal mass and inefficient heating direction (from inside to outside), Chen et al. developed a transparent fuser roller model in a xerographic machine to reduce warm-up time and energy [42]. The roller is made of a transparent Pyrex glass cylinder with black Teflon coating outside and a filament coil inside. Using a simplified Finite Element Method (FEM) model, a distributed, non-steady thermal fusing roller was analyzed with an ON/OFF and a fuzzy controller. This thermal model was further developed with a rubber-coated lower roller to model realistically [43]. For the best control-tools application, Simulink and PDE toolbox were used to run a simulation of the FEM model. The thermal model with the best controller, a P-controller, was implemented on a test bed, and thus proved to be a feasible model to control the fusing process in the xerographic machine.

The fusing process using a hot fusing roller showed strong potential as a new heating alternative for the automated fiber placement. Hence, this fuser heating technique is directly applied to the fiber placement process with heating tool design changes and process modifications. The main difference in the two heating techniques is the heat transfer rate at the contact area of the heating tool and the target material. The paper contact area of the fusing roller is small, such that the heat interaction at the area is small. On the other hand, the towpreg contact area of the rigid heating tool can be much bigger. As a result, manufacturing speed of the composite towpreg can be increased. There are also size and weight advantages with reasonable costs from printer/xerographic parts database. Due to the numerous advantages of the rigid contact heating, it will be investigated as an alternative heating method in the fiber placement process.

2.3 Towpreg Compaction

Compaction force is one of the major parameters of the quality of a finalized composite part [26,39,40,45,54]. Pitchumani et al. [16] proposed that the quality and performance of the final product is directly influenced by the presence of voids, so that a consolidation process plays a pivotal role in the manufacture of high quality composite parts. Moreover, good consolidation is important for eliminating residual stresses and warpage in the product [13].

Carpenter and Colton [15] developed a one-dimensional, semi-empirical process model to describe the deformation and flow phenomena of a towpreg for the filament winding process. This model was used to predict the roller pressure to achieve the desired fiber volume fraction and thickness of the consolidated composite. The applied load was found to significantly affect the final thickness at 99% confidence level and void content at a 94% confidence level of the specimens. As fiber volume increases, the required compaction load also increases. With increasing winding speed, the load decreases due to shear thinning effects. However, the maximum winding speed was limited by the time that the towpreg material had to bond to the layers beneath.

Hulcher et al. [54] varied compaction force in a fiber placement process and found its effect on the film interleaf layers quantitatively. Through a four-ply peel testing for two different compaction forces, 1.11 kN and 1.33 kN, average strength of two specimen showed 3 kN/m of difference for the same test conditions except compaction force. These results quantitatively show that compaction force significantly affects the quality of the composite parts.

Even though composite manufacturing methods often use a pneumatically actuated compaction mechanism with a robotic machine for the composite manufacturing, the possible variations due to the system have yet been discussed in the literature. The variation may eventually cause non-consistent compaction force in a consolidation process of automated fiber placement. In fact, the errors in the compaction force were found due to the external disturbances, such as complex surface shape of a structure, speed changes at start/end tape-laying process, and robotic machine vibrations. They will be discussed in static and dynamic compaction sub-processes.

3 Modeling of a Towpreg

Heat transfer models of three heating candidates for composite fiber placement are analyzed and compared in this section. It is generally known that composite material has non-linear governing equations [1] and non-linear material behaviors [3,7]. To quantify physical response time and energy efficiency for these heat sources, a linear heat transfer analysis in one-dimension along the thickness of the tow is developed with uniform material properties. Since a target composite material is thin, the possibilities of non-linear governing equation and non-uniform material properties can be neglected.

3.1 Heat Transfer Analysis for Alternative Heat Sources

Curing temperature for the target material, Fiberite 977-2 Toughened Epoxy Neat Resin thermoset, is 177°C. It is also known that composite material temperature drops by non-isothermal consolidation at the contact point with a compaction roller [39], so that the desired temperature of the towpreg is set to 190°C, 9.6% higher than the curing temperature. The external heat source should have a higher temperature than the desired, because the transient temperature profile of a composite with respect to time shows that response time rate of the composite to reach the target temperature decreases rapidly. To find the optimum temperature of the external heat source, modified rise time, which means the time for the composite to reach 5% band of the target temperature, is introduced. Otherwise, the time for the composite to reach the external heat source temperature from the lower 5% band, is as much as the time to reach the lower 5%

from the initial temperature. As a result, manufacturing speed is very inefficient. Hence, the external heat source temperature is set to 200°C, which is 5% higher than the desired towpreg temperature. In addition, no thermal expansion inside the composite and an adiabatic condition at the bottom of the thermoset composite is assumed [11]. Thermal properties are chosen from the composite material handbook [50] as in Table 1.

Table 3. Specifications and Thermal Properties of a Towpreg Composite

Parameters	Values
Density (ρ)	1310 (kg/m^3)
Specific Heat (C_ρ)	557.7 (J/kg/°K)
Thermal Conductivity (k)	0.288 (W/ m^2/°F)
Thickness of Towpreg (L)	0.13 (mm)
Natural Convective Heat Transfer Coefficient (h)	10 (W/m^2/°C)
Ambient Temperature (T_∞)	20 (°C)

3.1.1 Gas Heat Source

Since the heating process near the point of application is assumed one-dimensional and linear with uniform material properties, it can be modeled with a simple partial differential equation and simple boundary conditions: adiabatic at the bottom surface and convective heat transfer from the top surface. Initial temperature (T_∞) is assumed, 20°C, throughout the thickness and an average forced convective air heat transfer coefficient ($\bar{h}_g$), 260 (W/m^2/°C), is chosen from [39]. Figure 7 shows a schematic of a composite towpreg heating with a convective gas.

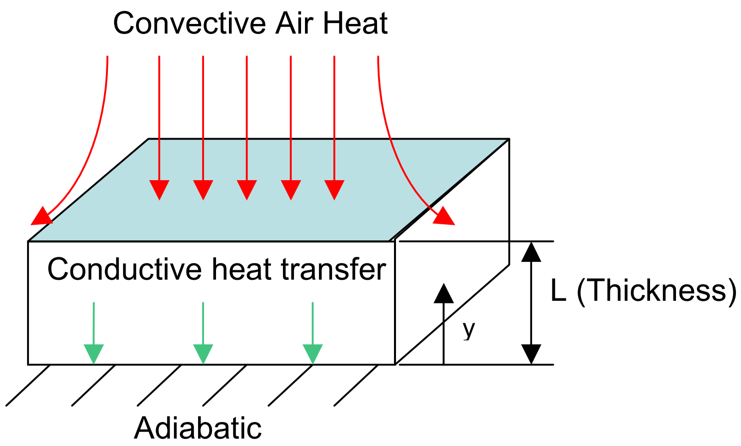

Figure 7. Schematic of Convective Gas Heat Input onto the Composite Surface

Partial Differential Equation:

$$\rho C_p \frac{\partial u(t,y)}{\partial t} = k \frac{\partial^2 u(t,y)}{\partial y^2} \qquad (1)$$

Boundary Conditions:

$$\bar{h}_g \left(T_{gas} - u(t,L)\right) = -k \left.\frac{\partial u(t,y)}{\partial y}\right|_{y=L} \tag{2–a}$$

$$-k \left.\frac{\partial u(t,\ y)}{\partial y}\right|_{y=0} = 0 \tag{2–b}$$

Initial Condition:

$$u(0,y) = T_\infty \tag{3}$$

where, $u(t,y)$ = Temperature of the composite material

t = Time

$\bar{h}_g$ = Average convective air heat transfer coefficient

T_{gas} = Constant gas temperature

T_∞ = Ambient temperature

By separation of variables [52], temperature distribution is easily calculated from the model. To change the nonzero boundary conditions to homogeneous ones, we try a solution of the form $u(t,y) = U(t,y) + w(t,y)$, where $w(t,y) = T_{gas}$. We could have two sets of partial differential equations for U(t,y) and w(t,y) as in Table 4. To apply the separation of variables method, we need to separate the PDE for U(t,y) into two ordinary differential equations. Substituting $U(t,y) = T(t)Y(y)$ into the PDE gives equation (4).

$$\dot{T}Y = \alpha^2 Y_{yy} T \quad \text{or} \quad \frac{\dot{T}}{\alpha^2 T} = \frac{Y_{yy}}{Y} \tag{4}$$

where, $\dot{T} = \dfrac{dT}{dt}$, $Y_{yy} = \dfrac{d^2Y}{dy^2}$, and $\alpha = \sqrt{\left(k \big/ \rho C_p \right)}$

Table 4. Partial differential equations (PDE), modified boundary conditions (BC) and initial conditions (IC) for U(t,y) and w(t,y)

PDE		$\dfrac{\partial U(t,y)}{\partial t} = \alpha^2 \dfrac{\partial^2 U(t,y)}{\partial y^2}$	$\dfrac{\partial w(t,y)}{\partial t} = \alpha^2 \dfrac{\partial^2 w(t,y)}{\partial y^2}$
BC	$y = 0$	$-k \left.\dfrac{\partial U(t,y)}{\partial y}\right\vert_{y=0} = 0$	$-k \left.\dfrac{\partial w(t,y)}{\partial y}\right\vert_{y=0} = 0$
	$y = L$	$\bar{h}_g\left(-U(t,L)\right) = -k \left.\dfrac{\partial U(t,y)}{\partial y}\right\vert_{y=L}$	$\bar{h}_g\left(T_{gas} - w(t,L)\right) = -k \left.\dfrac{\partial w(t,y)}{\partial y}\right\vert_{y=L}$
IC		$U(0,y) = T_\infty - T_{gas}$	$w(0,y) = T_{gas}$

Since the left-hand side depends on time and the right-hand side depends on y, both sides of the equation must be constants. Setting them both equal to $-\lambda^2$, we can have the two ordinary differential equations in (5-a,b).

$$\dot{T} + \alpha^2 \lambda^2 T = 0 \tag{5-a}$$

$$Y_{yy} + \lambda^2 Y = 0 \tag{5-b}$$

For the first equation, a general solution is $T(t) = e^{-\alpha^2\lambda^2 t}$. For the second equation, a general solution is $Y(y) = A\cos(\lambda y) + B\sin(\lambda y)$. By the modified boundary conditions in Table 4, B = 0 and $\tan(\lambda L) = \frac{\bar{h}_g}{\lambda k}$. Eigenvalues ($\lambda$) depend on the average convective heat transfer coefficient ($\bar{h}_g$) and do not depend on the gas heat source temperature (T_{gas}). The fundamental solutions are in equation (6), where each function of time and y-directional displacement satisfies the partial differential equation and the boundary conditions.

$$u(t,y) = w(t,y) + U(t,y) = T_{gas} + \sum_{n=1}^{\infty} A_n e^{-\alpha^2 \lambda_n{}^2 t} \cos(\lambda_n y) \tag{6}$$

Final step is applying an initial condition to the above equation.

$$(T_{\infty} - T_{gas}) = \sum_{n=1}^{\infty} A_n \cos(\lambda_n y) \tag{7}$$

To find the coefficients (A_n), each side of the equation must be multiplied by $\cos(\lambda_n y)$ and integrated from 0 to L.

$$A_n = \frac{2\int_0^L (T_{\infty} - T_{gas}) \cos(\lambda_n y) dy}{[\sin(2\lambda_n L)/2\lambda_n] + L} \tag{8}$$

The final analytical solution is obtained in equation (9).

$$u(t,y) = T_{gas} + \sum_{n=1}^{\infty}\left(\frac{2\int_0^L (T_\infty - T_{gas})\cos(\lambda_n y)dy}{[\sin(2\lambda_n L)/2\lambda_n] + L}\right)e^{-\alpha^2\lambda_n^2 t}\cos(\lambda_n y) \qquad (9)$$

For example, the first six eigenvalues (λ) are listed in Table 5 for the average convective heat transfer coefficient ($\bar{h}_g$) of 260 ($W/m^2/°C$), the constant gas temperature (T_{gas}) of 200°C, and towpreg thickness (L) of 0.2mm.

Table 5. Eigenvalues (λ) and Coeffiecients (A_n) of a Composite Towpreg Model with 0.2mm Thickness (L) and an Average Forced Convective Heat Transfer Coefficient ($\bar{h}_g$) for Hot Air Heating

n	1	2	3	4	5	6
Eigenvalues (λ_n)	2063	15990	31560	41960	52420	62880
Coefficients (A_n)	-185.1	6.24	-1.62	0.73	-0.41	0.26

The temperature profile at every 0.013mm elevation (y) versus time (t) for thickness (L) of 0.2mm is plotted in Figure 8. The response time for composite towpreg to reach 190°C for different thickness associated with given conditions is listed in Table 6.

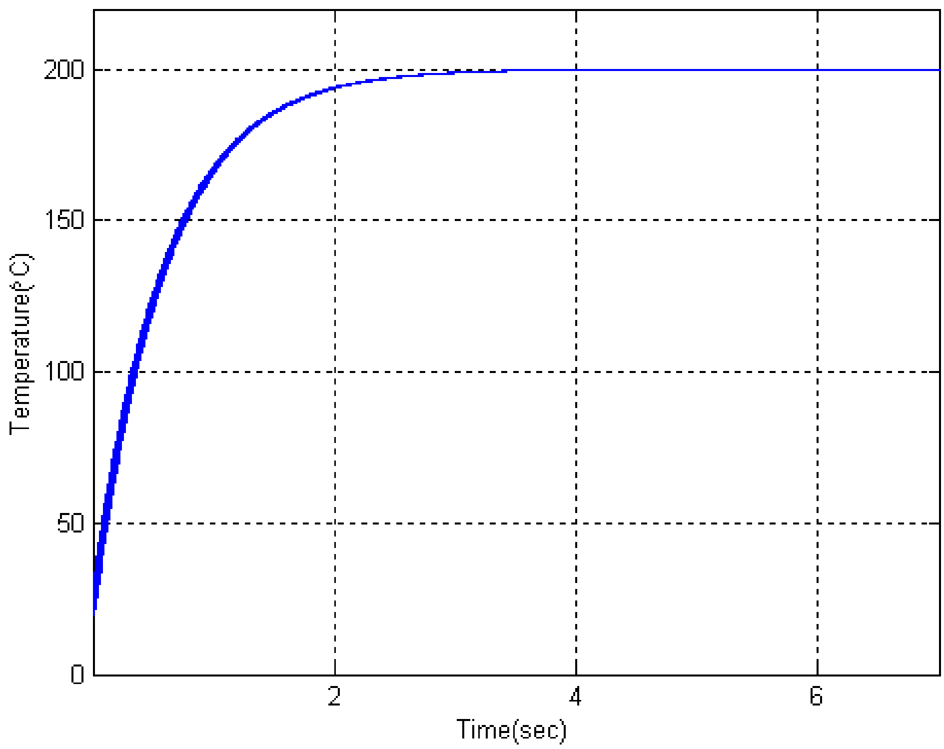

Figure 8. Temperature Profile at every 0.013mm Elevation to y-direction for 0.2mm Thickness and 200°C Convective Hot Air with $\bar{h}_g$ = 260 W/m^2/°C

Table 6. Response Time (sec) to reach 190°C with a Gas Heat Source, $\bar{h}_g$ = 260 W/m^2/°C and T_{gas} = 200°C for different Composite Thickness

Location	Composite thickness (L)			
	0.2 (mm)	0.3 (mm)	0.4 (mm)	0.5 (mm)
At top	1.69	2.58	3.50	4.45
At bottom	1.74	2.70	3.72	4.79

Response times vary significantly for different towpreg thicknesses (L). To find the main parameters of the response time for a gas heat source, a different hot air temperature (T_{gas}) and convective heat transfer coefficient ($\bar{h}_g$) are used to calculate response times from the model. First, response times for a different hot air temperature and tow thickness are plotted with the constant hot convective heat transfer coefficient, 260 ($W/m^2/°C$), in Figure 9. Three different convective hot air temperatures, 200°C, 250°C and 300°C, are applied onto the surface of thermoset towpreg as a boundary condition in equation (2-a). The resulting response times are much different as in Table 7. Hence, hot gas temperature (T_{gas}) is also a major contributor to composite material response time. Second, different convective air heat coefficients for different towpreg thickness are applied with the same hot air temperature, 200°C. This affects the response time substantially as shown in Figure 10 and Table 8. Therefore, composite tow thickness (L), hot air temperature (T_{gas}), and convective gas heat coefficient ($\bar{h}_g$) are sensitive parameters for thermoset response time.

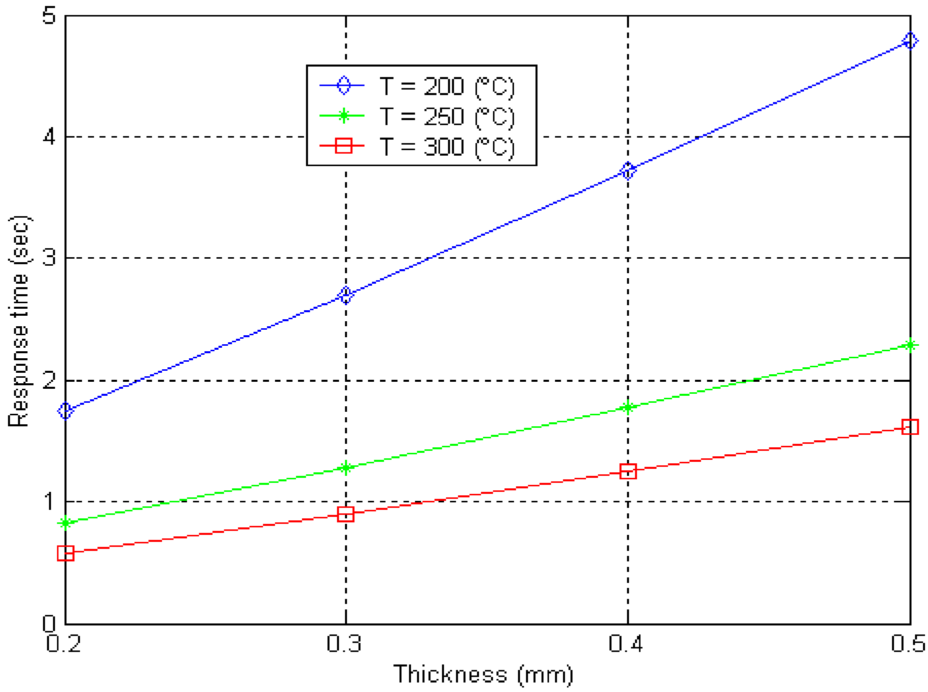

Figure 9. Response Time to reach 190°C for different Hot Gas Temperature (T_{gas}) with constant Convective Heat Transfer Coefficient ($\bar{h}_g$), 260 $W/m^2/°C$

Table 7. Response Time (sec) to reach 190°C at the Bottom Surface for different Convective Hot Air Temperatures (T_{gas}) with constant Convective Heat Transfer Coefficient ($\bar{h}_g$), 260 $W/m^2/°C$

T_{gas} (°C)	Composite thickness (L)			
	0.2 (mm)	0.3 (mm)	0.4 (mm)	0.5 (mm)
200	1.74	2.70	3.72	4.79
250	0.82	1.28	1.77	2.29
300	0.58	0.90	1.25	1.62

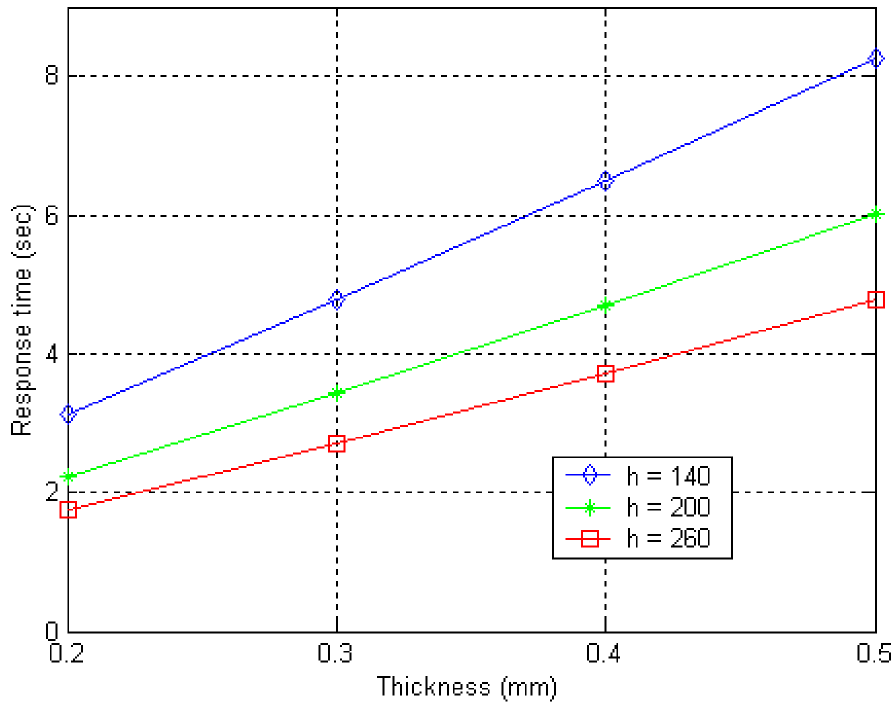

Figure 10. Average Response Time (sec) for different Convective Heat Transfer Coefficient ($\bar{h}_g$) with constant Hot Air Temperature of 200°C

Table 8. Response Time (sec) at the Bottom Surface for different Convective Heat Transfer Coefficient ($\bar{h}_g$) with constant Hot Air Temperature of 200°C

$\bar{h}_g$ (W/m^2/°C)	Composite Thickness (L)			
	0.2 (mm)	0.3 (mm)	0.4 (mm)	0.5 (mm)
140	3.14	4.79	6.50	8.27
200	2.23	3.43	4.69	6.01
260	1.74	2.70	3.72	4.79

3.1.2 Liquid Heat Source

A liquid heat source model is the same as a gas heat source model, but the convection heat transfer coefficient is generally much higher than that of a gas. Assumptions include uniform liquid properties and constant hot liquid temperature for all transient processes. Other process assumptions are that the liquid should be non-volatile for working temperature range and chemically non-reactive with the composite to be heated. Ideally, it should be environmentally non-toxic and relatively cheap.

According to Incropera [49], a convection heat transfer coefficient of forced liquid is typically at least two times higher than a coefficient of a forced gas, so that the average convective heat transfer coefficient ($\overline{h}_{\ell}$) with slow liquid-flow rate is assumed twice that of the convective air coefficient ($\overline{h}_g$) in previous section, 3.1.1. The calculated results of equations from (1) to (3) with constant hot liquid temperature (T_{liquid}) are quantified in Table 9 for several composite thicknesses (L).

Table 9. Average Response Time (sec) to 190°C with Liquid Heat Source, $\overline{h}_{\ell}$ = 500 W/m²/°C and T_{liquid} = 200°C

Location	Composite Thickness (L)			
	0.2 (mm)	0.3 (mm)	0.4 (mm)	0.5 (mm)
At top	0.91	1.41	1.94	2.49
At bottom	0.97	1.53	2.16	2.85

3.1.3 Rigid Heat Source

Equations (1) and (2) are the same as for a gas heat source except for boundary conditions, as in Figure 11. So, the same process with different boundary conditions (10-a,b) is used to find the temperature distribution inside the composite for a rigid heat source.

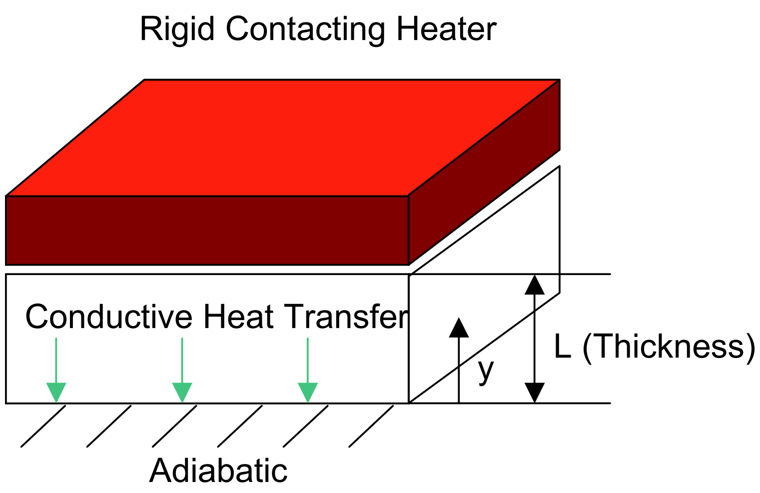

Figure 11. Schematic of Conductive Contact Heat Input onto the Composite Surface

Boundary Conditions:

$$-k\left.\frac{\partial u(t,y)}{\partial y}\right|_{y=0} = 0 \tag{10-a}$$

$$u(t,L) = T_{contact} \tag{10-b}$$

where, $T_{contact}$= Constant hot rigid heater temperature

A solution of the form $u(t,y) = U(t,y) + w(t,y)$ is tried to solve the partial differential equation, where $w(t,y) = T_{contact}$. Using the same process in section 3.2.1, eigenvalues (λ) are found in equation (11).

$$\lambda_n = \frac{(2n-1)\pi}{2L}, \qquad n = 1,2,3... \tag{11}$$

The fundamental solutions are in equation (12), and equation (13) is obtained by applying an initial condition to the equation.

$$u(t,y) = w(t,y) + U(t,y) = T_{contact} + \sum_{n=1}^{\infty} A_n e^{-\alpha^2 \lambda_n^2 t} \cos(\lambda_n y) \tag{12}$$

$$(T_{\infty} - T_{contact}) = \sum_{n=1}^{\infty} A_n \cos(\lambda_n y) \tag{13}$$

Multiplying $\sin(\lambda_n y)$ at each side of equation (13) and integrating from 0 to L, the coefficients (A_n) are calculated in equation (14).

$$A_n = \frac{2}{L}\int_0^L (T_{\infty} - T_{contact}) \cos(\lambda_n y)\, dy \tag{14}$$

As a result, the final analytical solution is calculated in equation (15).

$$u(t,y) = T_{contact} + \sum_{n=1}^{\infty}\left[\frac{2}{L}\int_0^L (T_\infty - T_{contact})\cos(\lambda_n y)dy\right]e^{-\alpha^2\lambda_n^2 t}\cos(\lambda_n y) \qquad (15)$$

The first six eigenvalues (λ) are listed in Table 10 for the constant hot rigid contact temperature ($T_{contact}$) of 200°C and towpreg thickness (L) of 0.2mm.

Table 10. Eigenvalues (λ) and Coeffiecients (A_n) of a Composite Towpreg Model with 0.2mm Thickness for a Rigid Contact Heat Source

n	1	2	3	4	5	6
Eigenvalues (λ_n)	7854	23560	39270	54980	70690	86390
Coefficients (A_n)	-229.2	76.39	45.84	32.74	-25.47	20.84

Temperature profile with a constant hot rigid contact temperature ($T_{contact}$) at each elevation (y) versus time (t) is plotted in Figure 12 for towpreg thickness (L) of 0.2mm. The calculated results with a constant hot rigid contact temperature are quantified in Table 11 for each composite thickness.

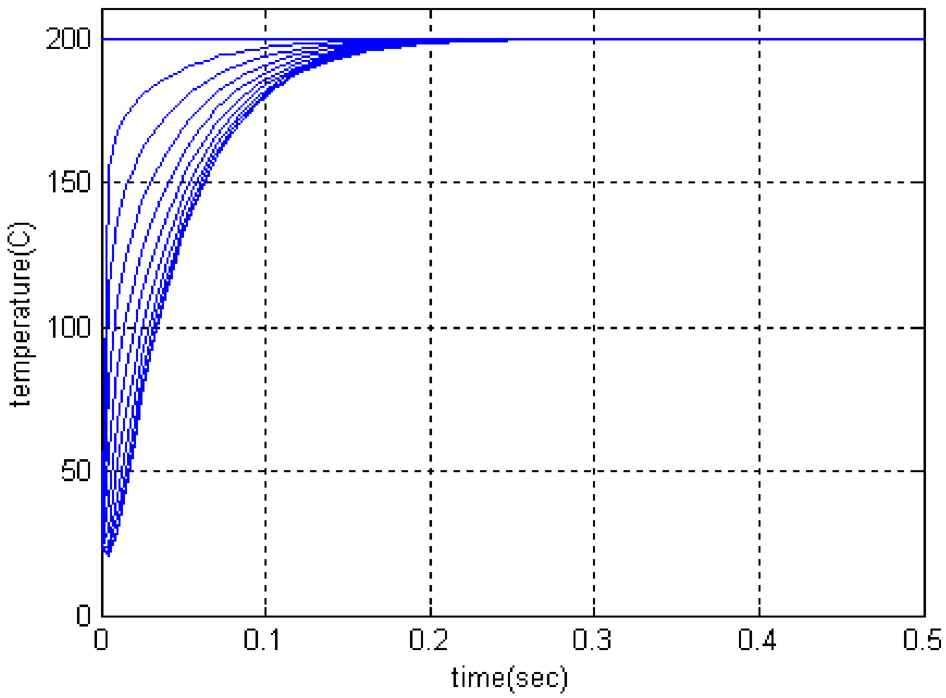

Figure 12. Temperature Profile at every 0.013mm elevation to y-direction for 0.2mm Thickness and a 200°C Rigid Contact Heating

Table 11. Average Response Time (sec) to 190°C with a Rigid Heat Source, $T_{contact}$ = 200 °C

Location	Composite Thickness (L)			
	0.2(mm)	0.3(mm)	0.4(mm)	0.5(mm)
At top	0	0	0	0
At bottom	0.13	0.29	0.52	0.81

3.1.4 Comparison of Heat Source Concepts

To compare manufacturing efficiencies of a composite towpreg with different heat sources, manufacturing speeds are calculated with the same towpreg specifications and effective heating area (A). Additional assumption is that the towpreg is moving linearly through the effective heating area, so that the results in chapter 3.1.1 to 3.1.3 are used to quantify the speeds. Since the effective heating area of the towpreg is assumed to be 1×1 cm^2, the maximum manufacturing speed for each heat source is calculated as a 1cm of length divided by a rise time of the towpreg with each heat source to reach the target temperature of 190°C.

The rigid contact heating has the shortest response time for the same process conditions with a constant heat source temperature, so that its manufacturing speed is the fastest in Table 12. For example, when a hot air torch with an effective heating area 1×1 cm^2 on the tow is used to heat the 0.2mm thick and 0.635cm wide composite tow, its manufacturing speed is at most 0.58cm/s to heat the composite tow up to the lower 5% target temperature band, 190°C. On the other hand, manufacturing speeds for liquid and rigid contact are 1.03cm/s and 7.69cm/s respectively to achieve the same condition. The rigid heat source is predicted at least 13 times faster than an air heat source and 7 times faster than a liquid heat source for the same effective heating area. Moreover, increasing the rigid contact surface of composite towpreg can increase effective heating area for more efficient towpreg heating.

Table 12. Manufacturing Speed (cm/sec) of the Composite for different kinds of Heat Inputs to reach 190°C. External Heat Source Temperature is fixed at 200°C and Effective Heating Area (A) of 1×1 cm^2

Input heat source	Composite Thickness (L)			
	0.2 (mm)	0.3 (mm)	0.4 (mm)	0.5 (mm)
Convective air with $\bar{h}_g$ = 260 (W/m^2/°C)	0.58	0.37	0.27	0.21
Convective liquid with $\bar{h}_\ell$ = 500 (W/m^2/°C)	1.03	0.65	0.46	0.35
Conductive solid with constant temp, 200°C	7.69	3.45	1.92	1.24

To compensate for the slow manufacturing speed with a hot gas heating, the temperature of the gas-heating tool is increased in the composite manufacturing processes [39,40]. Since the hot gas temperature is one of the main parameters of interest for the towpreg heating, the increased temperature, of course, can increase the composite manufacturing speed. For instance, a 0.2mm thickness towpreg is heated with different hot gas temperatures but the same convective heat transfer coefficient ($\bar{h}_g$). The manufacturing speeds are 0.58cm/sec for a hot gas temperature (T_{gas}) of 200°C and 7.41 cm/sec for the hot gas temperature of 1000°C.

However, the sensitivity at the target temperature of the towpreg is also increased. The tolerance of heating time, ±0.01 seconds, can change the towpreg temperature to ±13.4°C from the target temperature of 190°C, and thus the error may affect the quality of the finalized composite. Pitchumani et al. [16] warned that polymer degradation is a cumulative effect of the exposure of the polymer matrix to elevated temperatures through the duration of the process, occurs throughout the process, and is particularly of concern at the tow surface, which is exposed to the hot gas streams from the torches. Therefore, the manufacturing speed for a constant hot gas heating tool temperature should be very accurately controlled. In comparison, the sensitivity of the towpreg with the rigid heat source is very low at 190°C. The temperature change for the tolerance of ±0.01 seconds is ±2.67°C. Even for a significant amount of excessive heating time, the towpreg temperature never exceeds the heat source temperature of 200°C; as a result, a rigid contact heating is a safe towpreg heating method.

In addition, conventional heating techniques have non-uniform heating over the heating area. A localized heat source with a finite heating area was applied around the consolidation point with non-uniform heat intensity for composite towpreg heating, such that the temperature profile for the surface of the composite has different distribution in the effective heating area [19]. For gas flow from a circular shaped heating tool, the center point has the highest heat intensity, and intensity decreases as radial distance increases. The problem of non-uniform heat intensity can be easily solved by rigid contact heating with a large contact area and a constant heat source temperature. Temperature uniformity has already been proven in a xerographic machine and a printer [42,43].

3.2 Energy Efficiency Analysis for Different Heat Sources

Heat transfer analysis for each heat source in Section 3.1 considered a static composite specimen. In this section, a dynamic analysis with moving tow is carried out to determine energy efficiency. To quantify physical results for these heat sources, a one-dimensional analysis along the thickness of the towpreg and a linear model with uniform material properties will be used again.

3.2.1 Gas Heat Source

A layout for on-line consolidation of composite with a gas heat torch is shown in the literature of [4]. The setup is used for experimental composite fabrication in many literatures [4,5,19,20,21,22]. To quantify energy efficiency, an Osram Serpentine type II heat exchanger's specification [51] is used to calculate total input energy in equation (16) with some reasonable material properties from Section 3.1. Ambient temperature (T_∞) and constant hot air temperature (T_{gas}) are used to find the total power in heating from 20°C and 200°C respectively. Then total energy from the electric heating core (q_s) is calculated approximately to be 216 (W) with 50 SCFH airflow rate through the hot gas torch. When the effective heating area (A) onto the composite tow is set to 1×1 cm^2, heat input into the composite towpreg (q), whose width is 0.625cm and speed is 0.3049 cm/sec, is calculated 1.42 Watt by the convection heat transfer equation in (17). This model shows the energy efficiency (q/q_s) for air heat source is 0.66% of total heat input from electric heater core inside the hot air torch.

$$q_s = \frac{Q_g \times \left(T_{gas} - T_\infty\right) \times 1.2}{180000} \qquad (16)$$

$$q = \overline{h}_g A\left(T_{gas} - \overline{T}\right) \qquad (17)$$

where, Q_g = Hot air flow rate (SCFH)

q_s = Total energy from the electric heating core

q = Heat input into the composite tow

$\overline{T}$ = Average temperature of the composite

3.2.2 Liquid Heat Source

Hot liquid flows through nozzle and then onto the composite tow along l_1 and l_2 region in Figure 13. Since the hot liquid flow speed is much faster than tow moving speed, we can assume convective heat transfer on a stationary flat surface with external flow. In general, a thermal boundary layer is developed along the flat composite tow. Using this boundary layer theory, the speed of hot liquid (U_∞) can be calculated. To quantify heat efficiency, liquid thermal properties are chosen from unused engine oil at 160°C in [48]. They are density (ρ) of 805 kg/m^3, dynamic viscosity (ν) of 5.6×10^{-6} m^2/s, thermal conductivity (k) of 0.132 W/m/°C, Prandtl number (Pr) of 84 and specific heat (c_p) of 2.483 kJ/kg/°C. Hot liquid flow is laminar and the composite length ($l_1 + l_2$) is 4cm with width 0.625cm. The forced oil average convective heat transfer coefficient ($\overline{h}_\ell$) was assumed to be constant 500 W/m^2/°C in Section 3.2.2. However, the actual convective heat transfer coefficient depends on the position (x) inside of $(l_1 + l_2)$. When the speed of composite tow is 2.19 cm/sec, liquid flow speed (U_∞) is calculated to be 2.56 m/sec by equation (18). By assuming flow depth 5 mm and flow width 1 cm to cover the composite towpreg, a hot liquid flow rate ($\dot{Q}$) is calculated 0.000128 m^3/sec. The unused engine oil has a very high heat capacity, such that applying energy into the hot liquid (q_s) to reach 200°C from an initial liquid temperature of 20°C is found by equation (19) to be as high as 46 kWatt.

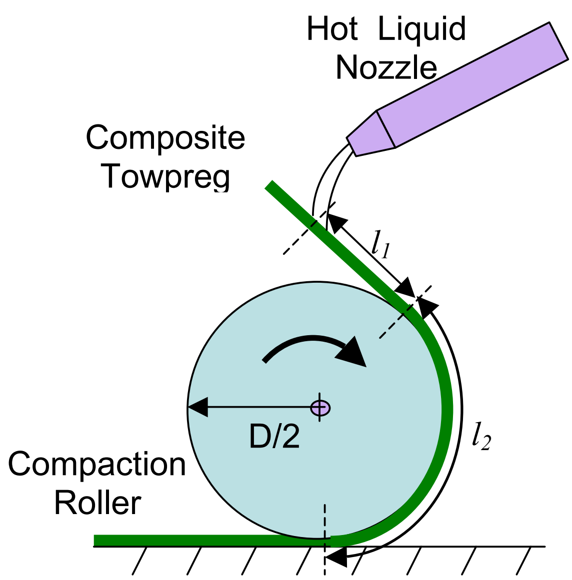

Figure 13. Schematic of Liquid Heat Source with Compaction Roller for Fiber Placement

$$\overline{h}_{\ell} = \frac{1}{(l_1 + l_2)} \int_0^{(l_1+l_2)} h_x dx \tag{18}$$

where, $h_x = \frac{Nu_x}{x/k}$

$$Nu_x = 0.451\sqrt{Re_x}\,Pr^{\frac{1}{3}}$$

$$Re_x = \frac{xU_\infty}{\nu}$$

ν = dynamic viscosity

$0 \leq x \leq (l_1 + l_2)$

Pr = Prandtl number

U_∞ = The speed of hot liquid

$\overline{h}_{\ell}$ = Average convective liquid heat transfer coefficient

$$q_s = \rho\dot{Q}c_p\left(T_{liquid} - T_\infty\right) \tag{19}$$

where, q_s = Applying energy into the hot liquid

$\dot{Q}$ = Hot liquid flow rate

T_{liquid} = Constant hot liquid temperature

Re-circulating the applied hot liquid and/or using a low heat capacity liquid can reduce the total heat input into the liquid. This improvement can be shown to reduce the energy input as low as 1 kWatt. Average temperature of the composite tow surface is calculated to be 156.5°C by equation (1,3) and modified form of (2).

The total energy absorbed in the tow (q) at the effective heating area (A) of 1×1 cm^2 is found by equation (20) to be 5.53 Watt. The energy efficiency of a liquid heat source is predicted to be 0.55% by the improved liquid heating.

$$q = \bar{h}_{\ell} A \left(T_{liquid} - \bar{T} \right) \tag{20}$$

where, q = Total energy absorbed in the tow

$\bar{T}$ = Average temperature of the composite

A = The effective heating area

3.2.3 Rigid Contact Heat Source

A model based on [42] is used to calculate the expected energy efficiency of rigid contact heating concept. The heating roller is assumed to have a very thin wall with uniform material properties and a thin coating of black Teflon. As with known copier terminology, radiation is used to heat the roller by a hot filament inside. An overall mechanical schematic is shown in Figure 14. To increase the heating contact surface for the composite tow, a separate compaction roller is used. Just after the composite tow leaves the heating roller, it starts to cool by natural air convection. So, the heating roller is positioned to minimize composite's contact surface with compaction roller so as not to lose energy by conduction into the compaction roller and convection into the air. For this model, the heating roller is 2.54cm in diameter; 2.54cm in length and the composite contact length (l_h) around the heating roller is 3cm for a width 0.625cm and thickness 0.3mm. By using the energy conduction equation in (21) with uniform material properties, we find the energy transferred into the composite tow (q) along the effective heating area (A) of 1×1 cm^2 is 30.27 Watt at a speed 16.95cm/sec. When the heating filament temperature inside heating roller and the target surface temperature is 1227°C and 200°C respectively, total energy from the filament (q_s) is 864 Watt by blackbody radiation assumption. Energy efficiency for rigid contact heat source is 9.23% for constant filament coil heat input.

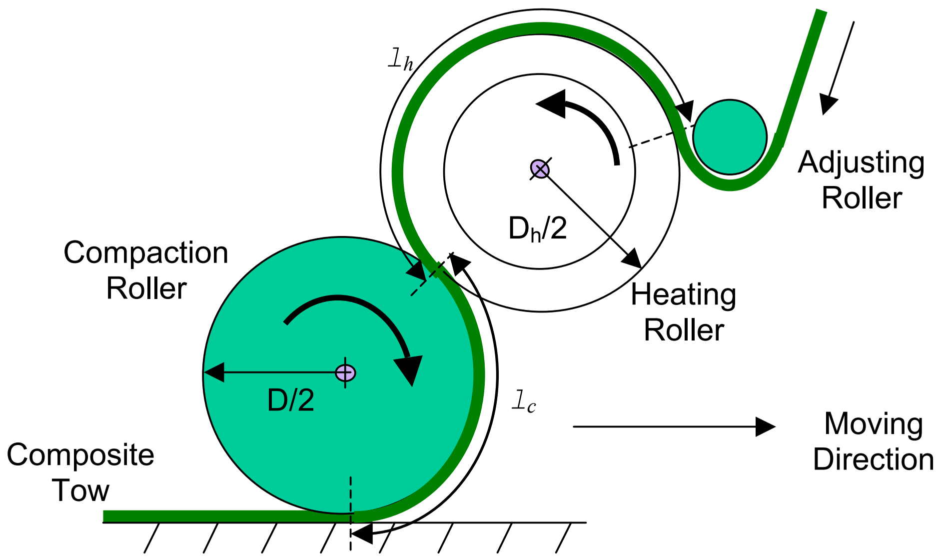

Figure 14. Schematic of Rigid Contact Heating with a Heating Roller for Fiber Placement

$$q = kA\frac{\left(T_{contact} - \overline{T}\right)}{L} \tag{21}$$

where, q = Total energy absorbed in the tow

$\overline{T}$ = Average temperature of the composite

A = Effective heating area

$T_{contact}$ = Constant temperature of the rigid contact heater

However, it should be clear that all the energy from filament coil should be stored into the composite tow or emitted into the air for energy balance. If this steady state condition does not hold, the surface temperature of the heating roller will rise higher than expected temperature 200°C. As a result, the heater coil might need to be controlled to keep the surface temperature constant. Heater coil control of the heating roller is well explained in [43] for transient and steady state conditions. Heating roller thickness is an important parameter in heating control. In case of a thin heating roller, response time to heat the roller to a desired temperature is very short, but the energy from the heating coil to the heating roller should be supplied consistently due to its small thermal mass. On the other hand, for the thick heating roller case, response time is slower, but the energy from the heating coil can be supplied intermittently due to its larger thermal mass.

4 Modeling of a Rigid Heating Roller in Contact with a Towpreg

A rigid contact heat source was found to be the most promising heat source in Chapter 3, and thus, it is further developed for modeling a composite heating process in automated fiber placement. A stationary roller model is first conceptually designed for static heating of the roller, and the roller model is used for quasi-static towpreg heating through direct contact. For static and quasi-static heating of a rigid roller, the PDE toolbox in Matlab Programming language version 6.1 [53] is used to run the simulation models. The PDE toolbox can generate a Finite Element roller model and run the simulation model with many kinds of controllers. For a Finite Element Method (FEM) application, a Matlab PDE toolbox is not an efficient tool due to its limited mesh generations and dimensional limitation. However, for control purposes, it is the best tool that can connect many controllers to the Finite Element model.

For quasi-static roller modeling in contact with a towpreg, the towpreg specifications in Section 3.1 are used except the towpreg thickness of 0.13mm. Since the temperature of the towpreg with the rigid contact heating is rising slowly with time, the modified rise time, meaning that the time for the towpreg to reach the lower 5% of the target temperature, is again introduced for efficient composite manufacturing. Hence, the target temperature of the towpreg is set at 190°C at the separation point.

4.1 Static Heating of a Rigid Roller

4.1.1 Modeling of a Static Rigid Roller

A linear two-dimensional roller model is developed to model the static heating of a rigid roller to target temperature, with respect to the radial and angular directions of the roller cross section as in Figure 15. A rigid roller is made of a hollow transparent Pyrex tube. The outside surface is coated with black Teflon and a heating lamp is located inside the roller. To quantify temperature profiles on the rigid roller surface, upon heating to the target temperature, uniform Pyrex and Teflon material properties are assumed and are presented in Table 13. A thin black Teflon coating is assumed to be 0.0245mm and has no thermal mass.

The radiant heat from the heating lamp inside the Pyrex roller is absorbed into the Teflon coating, and the heat is converted into heat flux at the outer boundary. No heat loss is assumed from the inner boundary of the roller. Both inner and outer boundaries of the roller are modeled with convective heat transfer. The target temperature of a rigid roller surface is 200°C. Towpreg width and roller length are both assumed to be 0.635cm. From a blackbody radiation assumption, 86.48% of the total power emitted by the lamp is transmitted to the black Teflon coating and absorbed by it [42,43]. The remaining 13.52% is absorbed by the transparent Pyrex roller, which is modeled as an evenly distributed heat source (Q) in equation (22). To model a rigid roller for static heating, the equations used are the same as the towpreg modeling in Section 3.1.1, except for thematerial properties, boundary conditions, and a two-dimensional temperature of the rigid roller (u) described in equations (23,24).

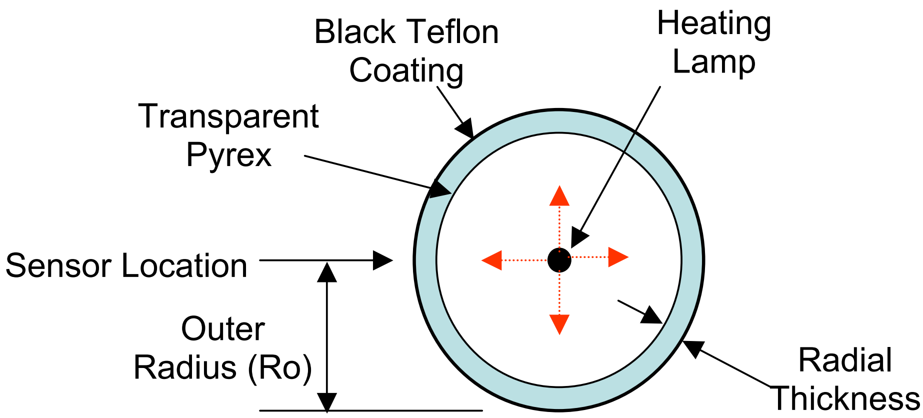

Figure 15. Schematic of a Rigid Heating Roller for Static Heating

Table 13. Specifications and Thermal Properties of a Static Rigid Roller

Parameters	Value
Roller Length	0.635(cm)
Outer Radius (Ro)	0.0252 (m)
Radial thickness of Pyrex tube	0.00155 (m)
Density of Pyrex (ρ)	2225 (kg/m^3)
Specific Heat of Pyrex (Cp)	835 (J/kg/°C)
Thermal Conductivity of Pyrex (k)	1.4 (W/m/°C)
Ambient Temperature (T_∞)	20 (°C)
Maximum Lamp Power	950 (W)
Natural Convective air heat transfer coefficient (h)	10 ($W/m^2/°C$)

Partial Differential Equation:

$$\rho C_p \frac{\partial u(t,x,y)}{\partial t} - \nabla \cdot [k \nabla u(t,x,y)] = Q \qquad (22)$$

Boundary Conditions:

$$\begin{cases} r = R_i, & n \cdot (k \nabla u) = 0 \\ r = R_o, & n \cdot (k \nabla u) = q - h(u - T_\infty) \end{cases} \qquad (23)$$

Initial Condition:

$$u(0,x,y) = T_\infty \qquad (24)$$

where, u (t,x,y) = Temperature of the rigid roller

t = Time

Q = Heat source

q = Heat flux due to radiant heating

n = Normal unit vector of the geometry boundary

A stationary sensor measures the temperature of the far left point of the roller surface, such that it is used for a feedback signal into a controller with the target temperature. Lamp dynamics is included with a time constant of 3.33 seconds in the simulation model in Figure 16. The radiant lamp inside the rigid roller is assumed to have a maximum power of 950 Watt. This maximum lamp output power is modeled by a controller output associated with a non-linear saturation function block in a simulation diagram, such that higher than 1 of the controller output signal results only in the maximum power of the lamp.

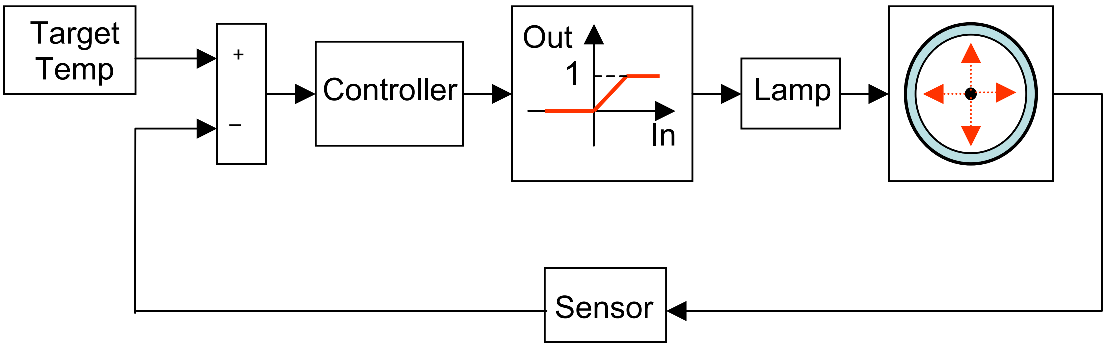

Figure 16. Simulation Diagram for a Static Rigid Roller Heat Control

4.1.2 Simulation Results

A minimum capacity controller, an ON/OFF controller, was employed in order to control the surface static rigid roller to reach the target temperature of 200°C. The temperature profile of the rigid roller surface was plotted in Figure 17. Temperature overshoot is 45.68°C and rise time is 0.32 seconds for the minimum feasible controller. Furthermore, the temperature profile with the controller shows that there is a steady state error of 3.17°C after 7 seconds of roller heating. Due to the high overshoot and the steady state error, the ON/OFF controller is not efficient controller for the static rigid roller heating. Hence, another candidate controller, a Proportional (P) controller, is employed to run the rigid roller heating simulation. The difficulty of this controller is how to pick out a proportional coefficient (Kp) that can achieve an efficient temperature rising with a low overshoot. Since the rigid roller model used is a distributed FEM system with 1200 of nodal points, a systematic way to find optimum coefficient is not available. Hence, by changing the coefficient from small to large number, the optimum coefficient was estimated as Kp of 0.01. As a result, the roller model with an optimum P controller was calculated, and the results were plotted in Figure 17. The results show that a temperature overshoot is 3.31°C and a rise time 0.42 seconds with the P controller.

Other controllers, such as a Proportional Derivative (PD) controller and Proportional Integral Derivative (PID) controller, were tried for better results for the same static rigid roller model. However, the temperature profile with the P controller did not have a significant temperature gradient with time, such that the distributed roller model was not sensitive to a Derivative component in the PD controller. Furthermore, since the results with the P controller did not have a steady state error after 7 seconds, the Integral component in the PID controller, did not affect the roller model, either. Therefore, the P controller with a proportional coefficient of 0.01 was concluded an optimum controller for the static rigid roller model.

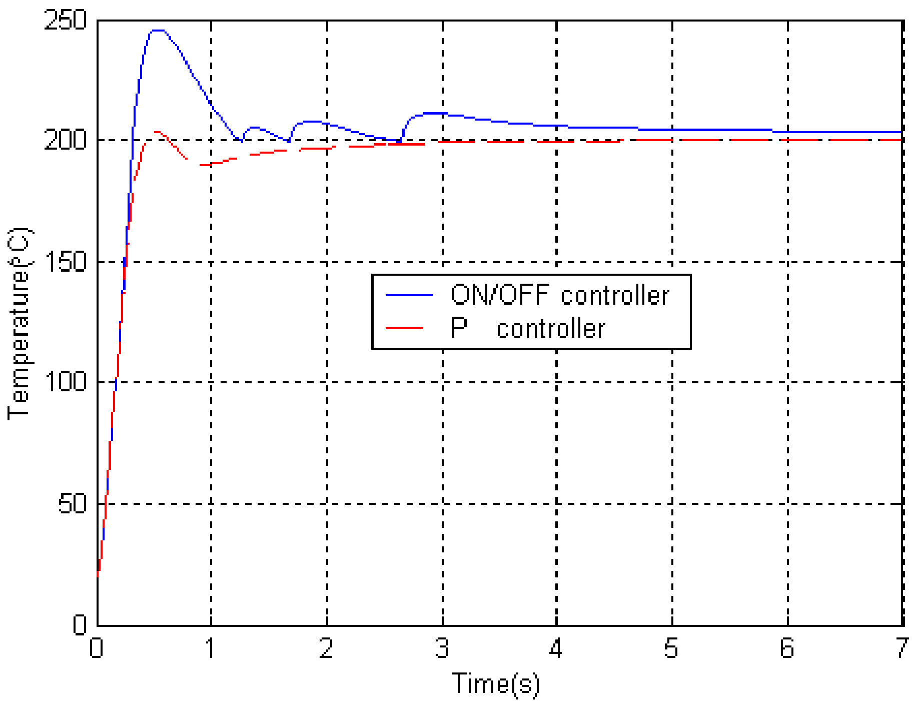

Figure 17. Temperature Profiles at the Outer Surface for Stationary Roller Heating with an ON/OFF Controller and a P Controller

4.2 Quasi-static Heating of a Rigid Roller in Contact with a Towpreg

The schematic of quasi-static heating of a rigid roller in contact with a composite towpreg is shown in Figure 18. Since the incoming towpreg has a rolling contact with the rigid contact-heating roller, the temperature of the towpreg increases as the contact time increases. The same thermal properties and specifications of the rigid roller in Section 4.1 are used to run the simulation of the quasi-static roller model. In addition, dynamic specifications and thermal properties for the quasi-static simulation are summarized in Table 14.

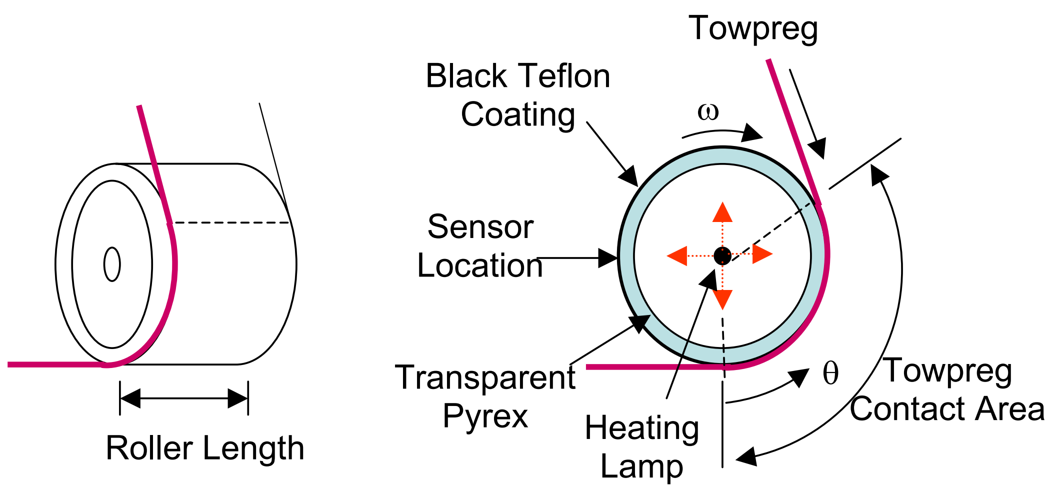

Figure 18. Schematic of a Rigid Heating Roller for Quasi-static Heating

4.2.1 Modeling of a Quasi-static Rigid Roller

To model quasi-static heating of a rigid roller in contact with a towpreg, the same model as that used for static heating was used, but with different initial conditions and boundary conditions. The temperature distribution at the end (t_1) of the static heating is used as an initial condition of a quasi-static heating of the roller model. Boundary conditions of the quasi-static model depend on the towpreg contact area, since the roller has rolling contact with the towpreg at the angular velocity (ω) of 20.94 rad/sec. Conductive heat transfer is modeled to describe the boundary conditions in the contact area between the roller and the towpreg, while natural convective heat transfer describes the boundary of the

Table 14. Specifications and Thermal Properties for a Quasi-static Rigid Heating Roller Model

Parameters	Value
Roller Length	0.635 (cm)
Outer Radius (Ro)	0.0252 (m)
Radial thickness of Pyrex tube	0.00155 (m)
Natural convective heat transfer coef. (h_d)	10 (W/m^2 /K)
Thermal Contact Conductance between a Pyrex tube and a Towpreg (h_{cp})	8086 (W/m^2 /K)
Angular Speed (ω)	20.94 (rad/s)
Sampling Rate of a Sensor	100 (Hz)

roller with no towpreg contact. However, since conductive heat transfer from or to a moving material with low thermal mass is difficult to model, the towpreg to roller interface is modeled as a convective heat transfer with a high thermal contact conductance (h_{cp}) at the interface as shown in [42,43].

An analytic towpreg model with different heat sources was developed in Section 3.1 with an adiabatic assumption at the bottom surface. For more realistic heat transfer modeling, the adiabatic boundary condition at the bottom surface is replaced with a natural convective boundary condition. This boundary condition change increases the heating time of the towpreg with a hot gas heating but does not change the heating time for rigid contact heating. For example, the rise time of a 0.13 mm thickness towpreg with the same gas heating conditions in Section 3.2.1 increases from 0.055 seconds with an adiabatic condition to 1.56 seconds with a natural convective condition. The rise times with the rigid contact heater are the same for different boundary conditions at the bottom surface. However, ratios of rise-time of the rigid contact heater to that of a gas heat source are significantly different for the boundary condition change. The rise time of rigid contact heating is at least 13 times faster for an adiabatic boundary condition and at least 28 times faster for a natural convective boundary condition than that of convective heating with the same convective heat transfer coefficient of 260 $W/m^2/K$. Hence, a thermal contact conductance (h_{cp}) that is marginally greater, 31 times, than the convective heat transfer coefficient, specifically 8086 $W/m^2/K$, is used to describe conductive heat transfer boundary conditions on the rigid roller. To simulate a rotating roller with a partial towpreg contact area, the boundary conditions are set to move around the roller surface at an angular velocity equal to the linear towpreg feeding velocity divided by the roller outer radius (Ro).

Partial Differential Equation:

$$\rho C_p \frac{\partial u(t,x,y)}{\partial t} - \nabla \cdot [k \nabla u(t,x,y)] = Q \qquad (25)$$

Boundary Conditions:

$$\begin{cases} r = R_i, & n \cdot (k\nabla u) = 0 \\ r = R_o, & \begin{cases} n \cdot (k\nabla u) = q - h_{cp}(u - T_{towpreg}) & \text{at towpreg contact area} \\ n \cdot (k\nabla u) = q - h_d(u - T_\infty) & \text{elsewhere} \end{cases} \end{cases} \qquad (26)$$

Initial Condition:

$$u(t_1, x, y) \qquad (27)$$

where, u(t,x,y) = Temperature of the of the rigid roller

t = Time ($t \geq t_1$)

t_1 = The end of a stationary roller heating up time

Q = Heat source

q = Heat flux due to radiant heating

n = Normal unit vector of the geometry boundary

$T_{towpreg}$ = Towpreg temperature in contact with the roller

A stationary sensor is positioned at 90 degrees from the towpreg separation point to the close-wise direction. The sensor measures the surface temperature of the roller with a sampling rate of 100 Hz, and, subsequently, the measured data are used in the feedback loop of the temperature controller. Because a heating lamp located inside the roller has the maximum power limitation, there is a non-linear saturation function block that can saturate the controller outputs. Passing through the saturation function block, the controller output signal is used to control the heating lamp. As a result, radiant energy from the lamp regulates the roller surface temperature. The quasi-static simulation diagram for the rigid heating roller in contact with the towpreg is shown in Figure 19.

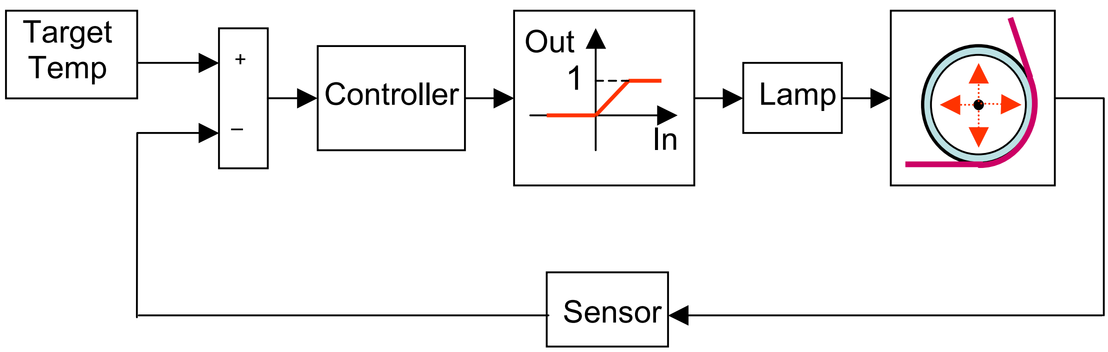

Figure 19. Simulation Diagram of a Rigid Heating Roller for Quasi-static Heating

In the roller towpreg contact model, the target temperature of the roller surface is 200°C and the angle of roller contact (θ) is assumed to be 120 degrees throughout the quasi-static heating area. For discrete finite element model simulation, the rigid roller has the same boundary condition values of within each

12-degree segment. At each time step of 0.01 seconds, the towpreg model is calculated with constant conductive boundary conditions, where the constant temperatures are roller surface temperatures. The averages of towpreg temperature profiles for 0.01 seconds are again used for the boundary conditions of a quasi-static heating roller model with a high thermal contact conductance (hcp). Both the rigid heating roller model and the towpreg model are solved simultaneously. Since the angle of roller contact (θ) is 120 degrees, a towpreg is heated for 0.10 second. The analysis speed represents a towpreg application rate of 33.38 cm^2/sec.

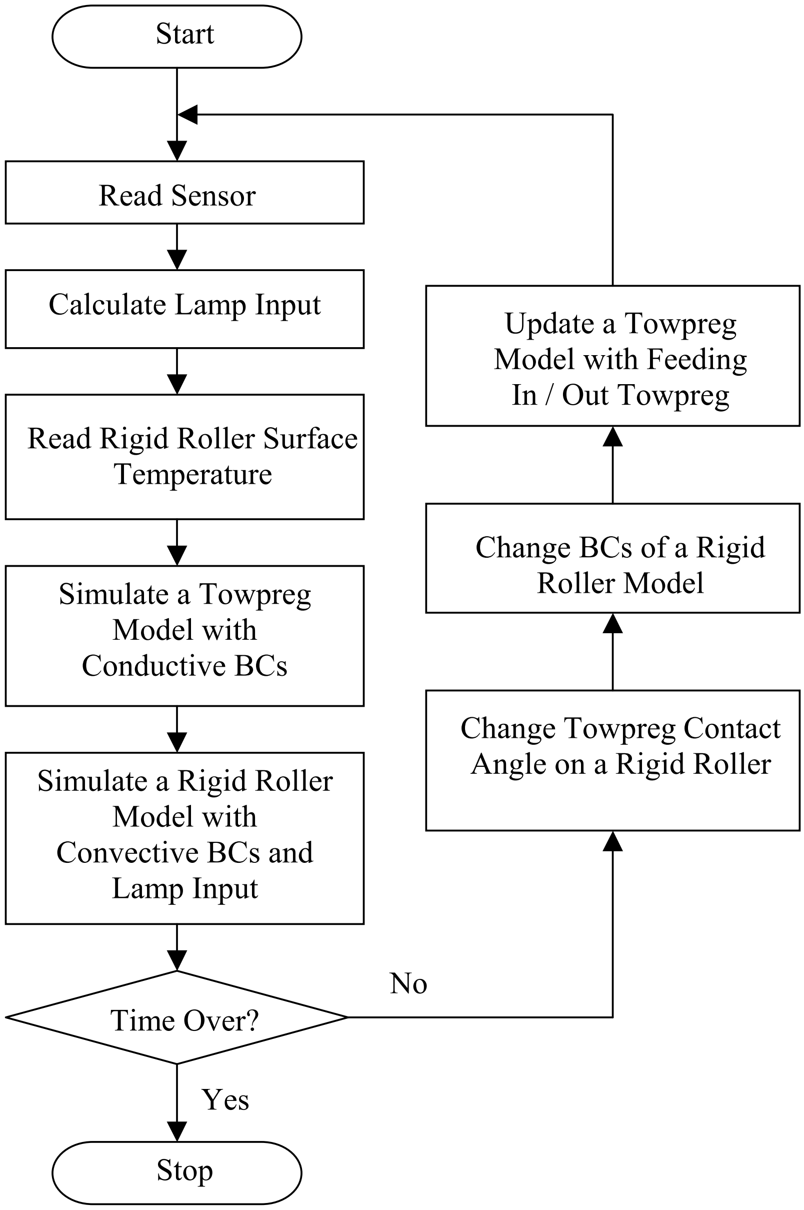

Figure 20. Algorithm Flowchart for a Quasi-static Heating of a Rigid Roller in Contact with a Towpreg

4.2.2 Simulation Results

Since the incoming towpreg and the rigid heating roller have a rolling contact, the towpreg temperature increases as the contact time increases in Figure 21. The P controller in section 4.2.1 was again employed to run a simulation of a quasi-static rigid roller model in contact with a towpreg. However, the temperature gradient at the towpreg contact area was very significant, so that, a new controller with a Derivative component (D) was required to effectively control the roller model. Thus, after varying the coefficients of a PD controller in the simulation diagram, a proportional gain (Kp) of 0.02 and a derivative gain (Kd) gain of -0.0001 were chosen to be optimum coefficients of the PD controller for the quasi-static heating of a rigid roller. Temperature profiles of the rigid roller surface

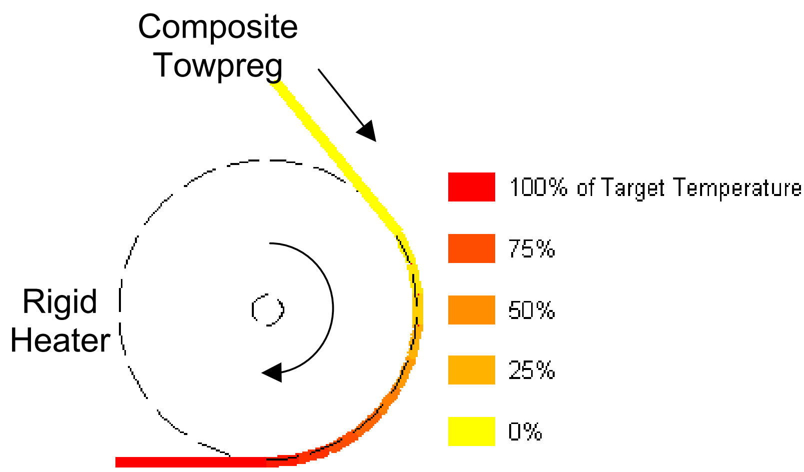

Figure 21. Temperature Dstribution of a Towpreg in Contact with a Rigid Heating Roller

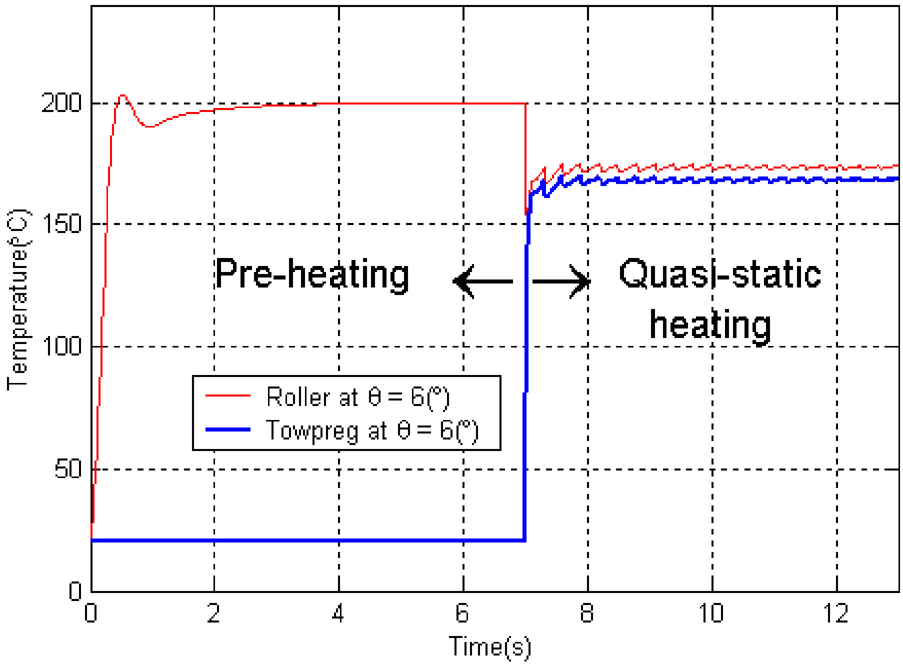

Figure 22. Temperature Profiles of a Roller Surface and a Towpreg with a PD controller

and the towpreg with the PD controller are plotted in Figure 22 for both preheating and quasi-static heating.

After 3 seconds of quasi-static heating of a rigid roller in contact with a towpreg, the average temperature of a towpreg reaches 167.8°C before separation from the rigid roller. The heated towpreg temperature is much less than the desired temperature of 190°C for a composite fiber placement. The lower temperature is a result of the difficulty for an omni-directional radiant heating lamp to keep uniform surface temperature on the rigid roller with non-uniform boundary conditions. The heat transfer rate of the rigid roller in contact with the towpreg is at least 800 times higher than the rate without the towpreg contact. The same amount of heating from one heating lamp results in either excessive surface temperature of non-towpreg contact area or lower surface temperature than desired. In addition, to avoid sensor touching to a hot towpreg that was placed on a subtrate, sensor location is necessarily far from the roller surface in contact with a towpreg. Even though the temperature drop rate at towpreg contact area is significant, the sensor could not measure temperature variation instantly. There is a 0.075 seconds delay due to the towpreg speed until a sensor reads a roller surface temperature difference. Additionally, there is 90 degrees of angle between the towpreg separation point and the sensor location on the rigid roller, so that roller surface temperature while the roller rotates 90 degrees recovers the target temperature. As a result, the average temperature is 204.9°C at the non-towpreg contact area and 173.1°C at the towpreg contact area before towpreg separation. To heat a towpreg up to 190°C, the target temperature of the rigid heater is increased systematically in Figure 23. When the target temperature is set to 230°C, the average towpreg temperature reaches 191.8°C.

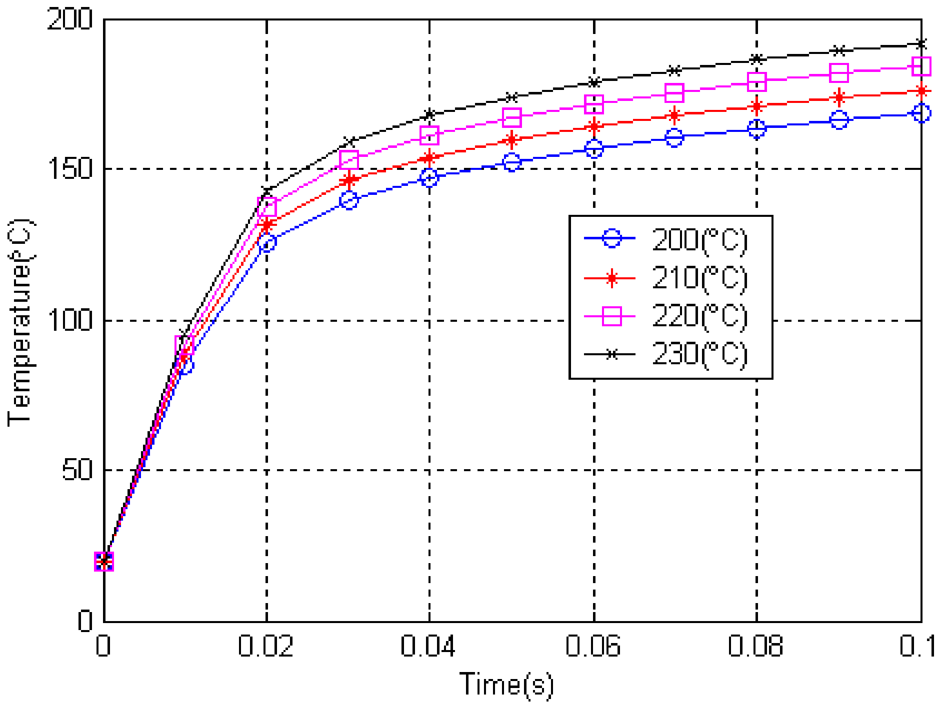

Figure 23. Average Temperature Profiles of a Composite Towpreg for the Target Surface Temperatures of a Rigid Roller with a PD controller

To find an optimum rigid roller specification, the outer radius (Ro) and the radial thickness were varied. Simulation results are summarized in Table 15 and Table 16 with a PD controller and a target temperature of 230°C. The minimum temperature of a composite towpreg after the quasi-static heating process must be at least 190°C and the fluctuations of the temperature profile should be as small as possible for uniform composite quality during fiber placement. The best roller specifications were found to be an outer radius (Ro) of 2.51cm and a radial thickness of 0.155cm with the PD controller. The temperature profiles of a towpreg and a rigid roller using the best parameters are plotted in Figure 24. The temperature of a composite towpreg was controlled at the minimum temperature of 190.7°C and within a 2.51°C of fluctuating temperature band.

In comparison, an ON/OFF controller is used for quasi-static heating, and an outer radius (Ro) and a radial thickness are varied with a target temperature of 230°C to find an optimum rigid roller specification in Table 17 and Table 18. The minimum temperature of a heated towpreg for an optimum specification is 8.1°C higher than the minimum with a P controller. However, the fluctuation band is increased to 4.03°C. For accurate heating of the composite towpreg, consistent temperature control is a foremost concern. Therefore, the P controller, which can more consistently control the towpreg, is a better controller.

Therefore, the rigid contact-heating roller with an optimum PD controller is a promising heating tool for a composite towpreg heating for its outstanding temperature controllability.

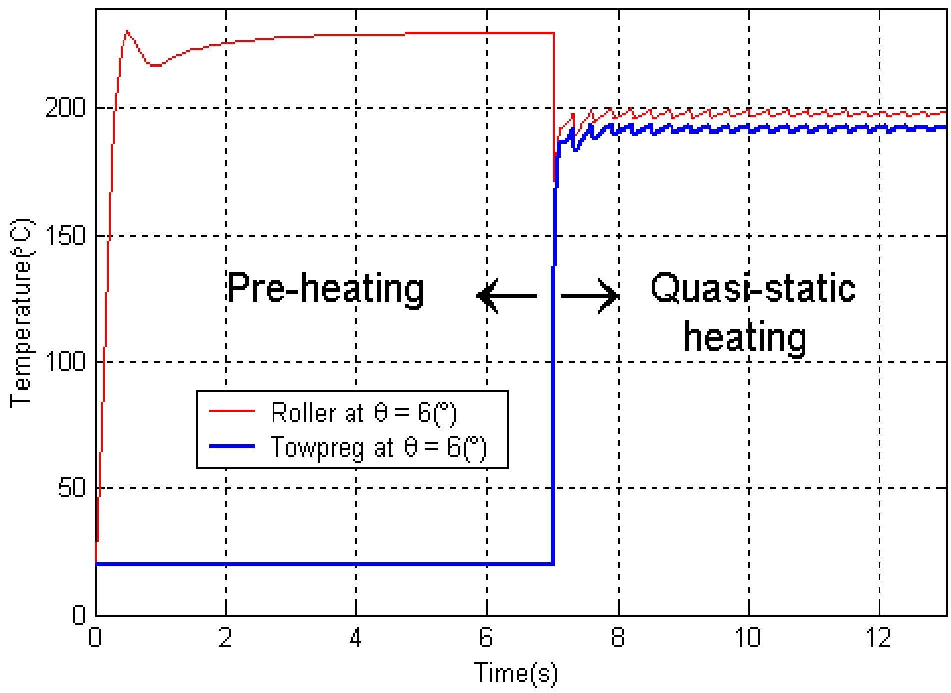

Figure 24. Temperature Profiles using the Best Parameters of an Outer radius (Ro) and a Radial Thickness with a PD controller

Table 15. Maximum Fluctuating Band (°C) of a Towpreg at the Angle of Roller Contact (θ) of 6 degrees with a PD controller

Ro (cm)	Radial thickness (cm)				
	0.124	0.155	0.186	0.186	0.248
1.76	11.02	10.52	3.61	3.61	4.02
2.01	3.04	11.25	10.73	10.73	4.22
2.26	2.98	11.91	11.44	11.44	4.19
2.51	7.88	**2.51**	11.06	11.06	17.82
2.77	6.91	2.64	11.61	11.61	11.15

Table 16. Minimum Temperatures (°C) of a Towpreg at the Angle of Roller Contact (θ) of 6 degrees with a PD controller

Ro (cm)	Radial thickness (cm)				
	0.124	0.155	0.186	0.217	0.248
1.76	191.1	194.2	193.7	194.6	195.6
2.01	191.6	192.5	195.6	193.6	194.6
2.26	190.9	191.5	194.4	196.2	194.0
2.51	188.4	**190.7**	193.2	195.5	196.7
2.77	188.3	189.9	191.9	194.1	195.7

Table 17. Maximum Fluctuating Band (°C) of a Towpreg at the Angle of Roller Contact (θ) of 6 degrees with an ON/OFF controller

Ro (cm)	Radial thickness (cm)				
	0.124	0.155	0.186	0.217	0.248
1.76	17.14	14.27	5.59	5.47	4.17
2.01	**4.03**	17.50	15.39	8.49	7.87
2.26	5.24	16.38	14.43	23.69	8.30
2.51	9.73	5.80	13.25	13.09	19.99
2.77	8.02	4.92	14.97	13.90	11.78

Table 18. Minimum Temperatures (°C) of a Towpreg at the Angle of Roller Contact (θ) of 6 degrees with an ON/OFF controller

Ro (cm)	Radial thickness (cm)				
	0.124	0.155	0.186	0.217	0.248
1.76	196.92	202.98	200.65	201.79	204.15
2.01	**199.77**	199.72	203.67	200.67	202.20
2.26	199.17	199.32	203.81	205.80	202.46
2.51	197.80	199.32	203.56	206.26	208.51
2.77	198.37	199.59	202.61	205.86	208.71

5 Compaction Force Analysis

A pneumatic compaction mechanism has frequently been used for applying compaction force in automated composite manufacturing [15,39]. As the demand for high quality composite structures increases, compaction force needs to be reinvestigated for possible variations in consolidation of placed fiber. Ideally, the pneumatic compaction mechanism driven by a robot, so called a compaction system, would give constant force in the presence of external disturbances such as arbitrary surface shape of a structure, start/end tape-laying, and machine vibrations. These disturbances may cause an undesirable effect during the compaction process unless the pneumatic compaction mechanism and the robot are accurately controlled. As shown in Figure 1, a non-consistent compaction force was found with the compaction system used for this research. The color of a 3.5 inch-long track in the figure indicated the compaction force was not uniform while the compaction system ran on a flat surface linearly with a constant speed. Since the pneumatic compaction system could not achieve a consistent compaction force, the compaction mechanism driven by the robot was studied in detail.

Compaction force will be investigated from two viewpoints. First, vertical motions of the pneumatic mechanism will be addressed for possible static force variations at each vertical position. Second, compaction force analysis for lateral motion of compaction mechanisms will be discussed. This analysis was again classified into static, steady dynamic, and unsteady dynamic force: (1) For static compaction force, a pneumatic mechanism with an air-cylinder was investigated for its possible variations under static and external load environment. In addition, two alternative compaction techniques using a spring only and a spring combined with an air-cylinder were suggested and compared with the conventional pneumatic compaction. (2) Steady dynamic compaction force was analyzed to quantify the overshoot component of force variation. Furthermore, it was attempted to quantify how fast the compaction mechanism was ready to move with a desired compaction force as well, because the time to reach the desired force with the compaction mechanism affects the manufacturing speed in a consolidation process. Fast rise time of the compaction force to the desired level is required for an efficient consolidation process, but an excessive force caused by an overshoot of the steady compaction force profile should be avoided. (3) An unsteady dynamic force was identified fluctuating throughout the compaction process by the compaction system. Through Fast Fourier Transform (FFT) analysis [69], the main reasons for the non-consistent dynamic unsteady compaction force will be discussed qualitatively and quantitatively in this chapter.

5.1 Experimental Setup

The goal of a compaction force analysis is to understand the physical phenomenon of the compaction process using a pneumatic mechanism and a robot, and furthermore, to find control variables of the compaction system. To achieve this goal, a Merlin Robot MR-6200 [59,60] was used to move the compaction mechanism. A sensitive force/torque sensor, JR-3 [56,57], was installed on the robotic endplate to measure the force. In addition, the compaction mechanism was comprised an air-compressor, an air-cylinder with a sequence controller, a relief valve, an air-pressure regulator, an aluminum end-effector, and a robotic workcell. With the robot and the force sensor, this compaction mechanism was used to apply compaction force which is directed normal to the worktable.

To visualize the compaction force, a thin tactile force/pressure sensor [55] was used in Figure 1. By placing the sensor film between a compaction mechanism and a worktable, this sensor could measure the pressure range of 350 – 1400 psi. It also can determine how the compaction force was distributed and what the pinpoint magnitude was while the mechanism moved on the sensor.

5.1.1 Merlin Robot

The MR-6200 used in the experiment is a six-axis, articulated robot with three major axes and three wrist axes. The major three axes are the waist, shoulder and elbow. The robot is also capable of three wrist motions – wrist rotate, wrist flex and hand rotate as shown in Figure 25. The robot has a reach of 40 inches and can carry a payload of 20 lbs. The resolution of the robot allows it to position the tool-tip within 0.001 inch of a previously defined point. The controller of the robot is designed for industrial use and can control up to 24 axes (or 4-six axis machines). The AARM motion controller is PC-based and can be run on either DOS or Windows NT. On DOS, the robot can be programmed in ARBASIC programming language while it can be run using either MS Visual C++ or Visual Basic on Windows NT.

The robot is capable of three basic types of motion – joint-coordinated, straight-line and circular motion. Joint-coordinated motion allows the arm to reach top speed consistently and allow moves that are not possible in straight-motion. In straight-motion, the robot traces a straight line from the start position to the goal. The robot traces a circular path when commanded to move in circular motion

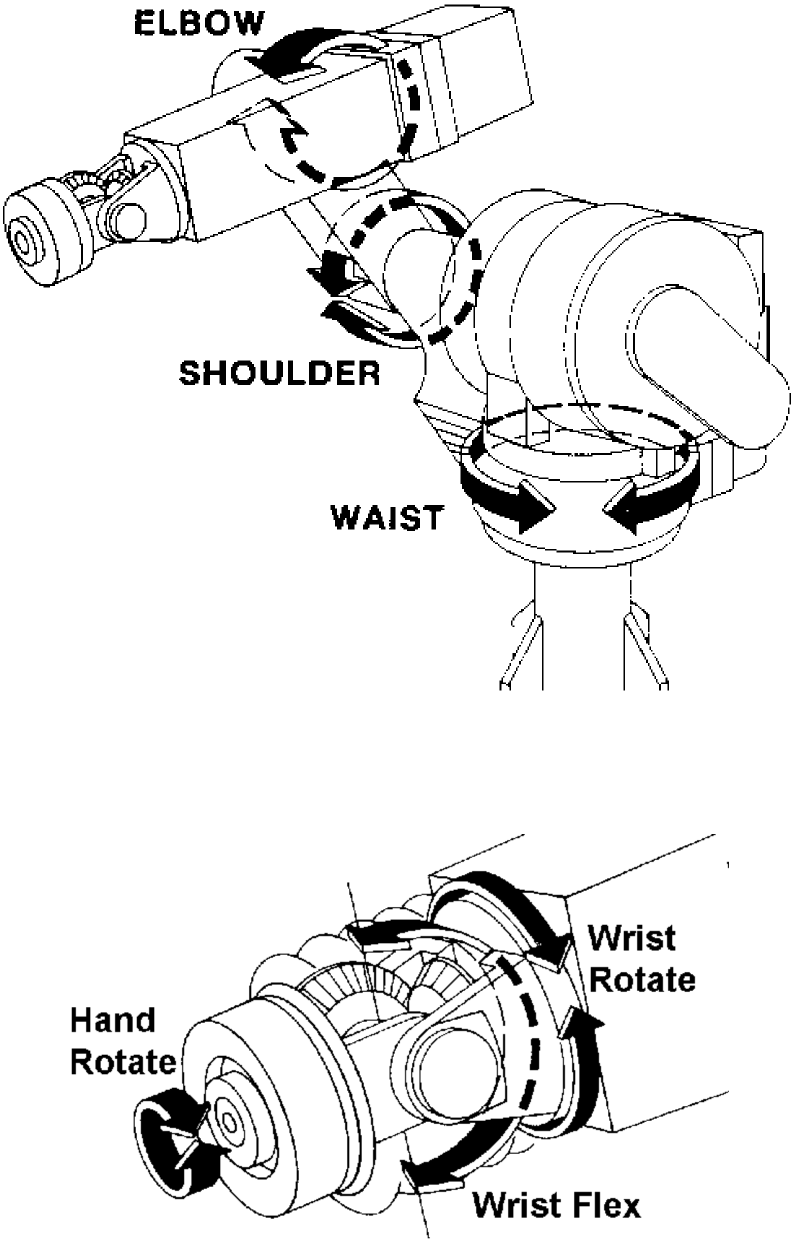

Figure 25. Schematics of the Merlin Robot 6200 with six-axes [60]

mode. This mode is useful when working on circular paths, such as welding and painting. In our experiment, straight-line mode was used to measure the compaction force under load.

5.1.2 Force/Torque Sensor, JR-3

The JR-3 force/torque sensor used is a six-axis device capable of measuring forces and moments in three directions to a precision of four decimal places. The force sensor uses DSP-based receiver with an IBM-AT bus interface. The software provided with the sensor is designed to run on a Window 95/98/2000 platform. User code can be written in either Visual Basic, Visual C++, or in any language that permits communications with external hardware. In order to use the force/torque sensor on an NT platform, a device driver that allows the operating system to communicate with the sensor is needed.

The JR-3 is installed on the robotic endplate for measuring the compaction force as shown in Figure 26. The JR-3 model is a 100M40A, whose dimensions are diameter of 100 mm, thickness of 40 mm with maximum load rating, 100 lbs. The compaction force was measured with respect to the center of the robotic endplate during the fiber placement process. The resolution of this force sensor, JR-3, was measured 0.00234 lb.

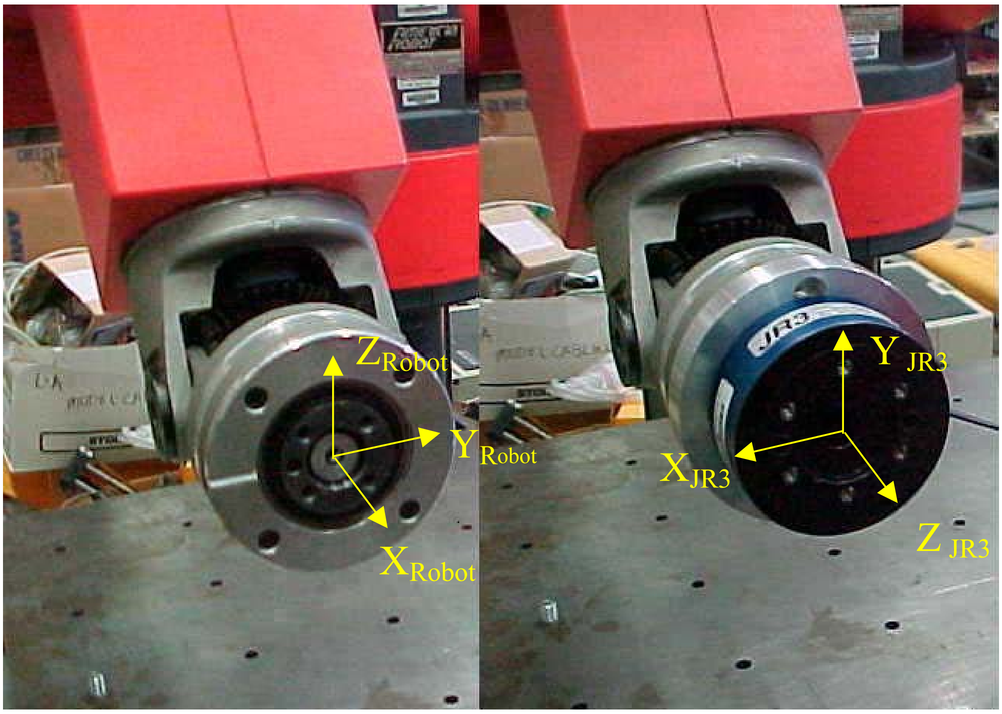

Figure 26. Robotic Endplate with Robotic Local Coordinates (Left); Robotic Endplate with a Force/Torque Sensor, JR-3, and Sensor Coordinates (Right)

5.1.3 Auxiliary Equipment

Air-pressure from an air-compressor was pre-regulated by a Wilkerson air-pressure regulator [71] and was controlled by a Norgren relief valve [72] installed at the inlet of an air-cylinder. The pressure range of the regulator and the relief valve shown in Figure 27 is from 0 to 125 psi at the maximum temperature of 79°C and 65°C respectively. The air-cylinder used is an 18-CSD-2 Heavy Duty Aluminum air-cylinder with a 1.125” Bore [70] and has a maximum stroke of 2 inches. To control the airflow direction to the air-cylinder, we designed a sequence controller as shown in Figure 28. The controller was connected to the computer that controls robot, so that the airflow to the air-cylinder and the robot motion can be simultaneously controlled. The computer used is a 233 MHz Pentium-MMX. We also designed an aluminum end-effector to use the cylinder in a compaction mechanism shown in Figure 29. Either a roller or a ball-caster component can be installed at the end of the piston rod, so that the pneumatic sequence controller can move it inward or outward of the cylinder by changing the airflow direction. The overall diagram of the compaction system is shown in Figure 30.

Figure 27. Wilkerson Air-pressure Regulator [71] (Left) and Norgren Relief Valve (Right) [72]

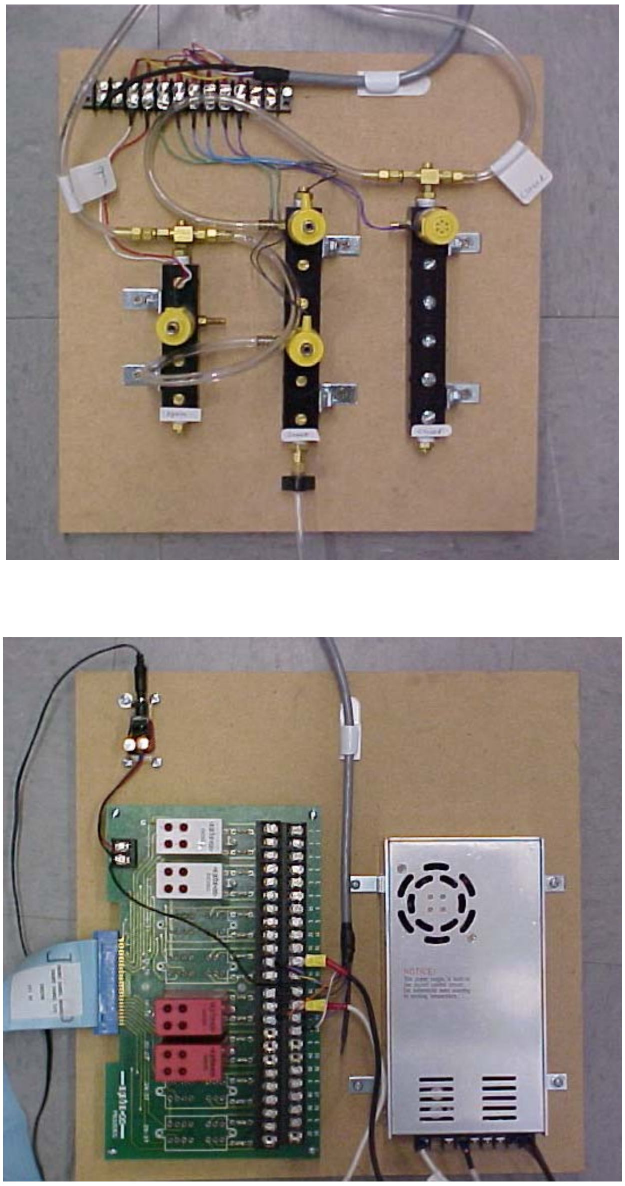

Figure 28. Sequence Controller (Top) and Sequence Control Board (Bottom)

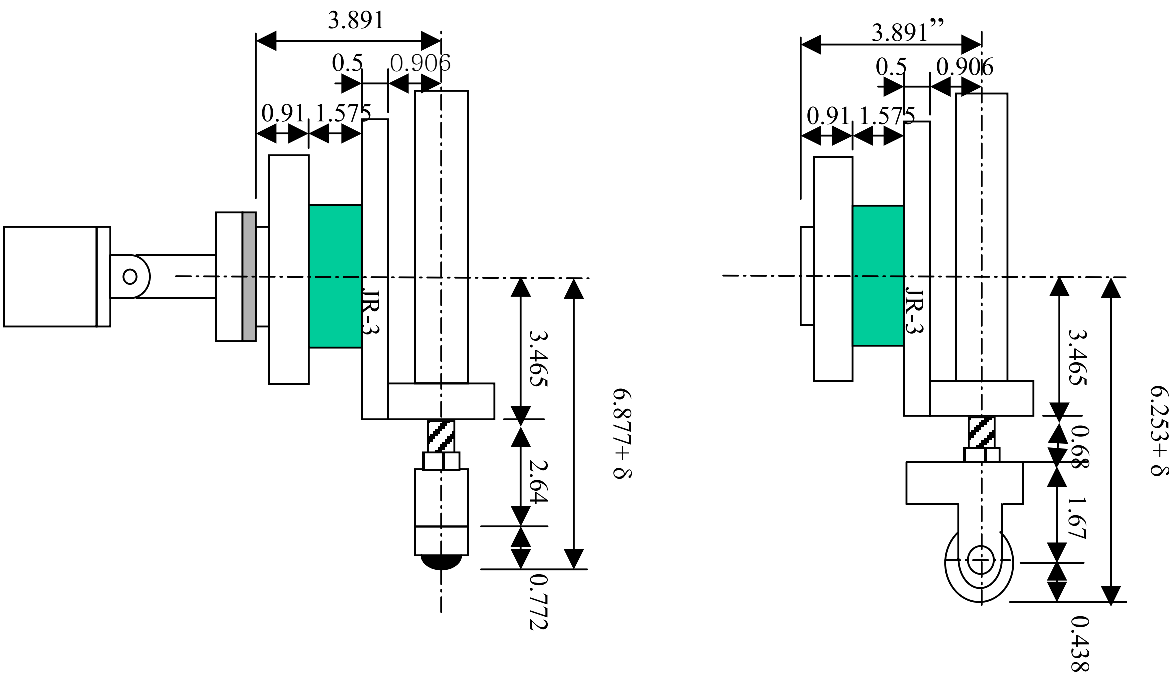

Figure 29. Schematics of a Robotic End-effector with a Roller and a Ball-caster: The stroke of the air-cylinder is 2.0 inches, so that the range is 0 ≤ δ ≤ 2.0 inches (unit: inch)

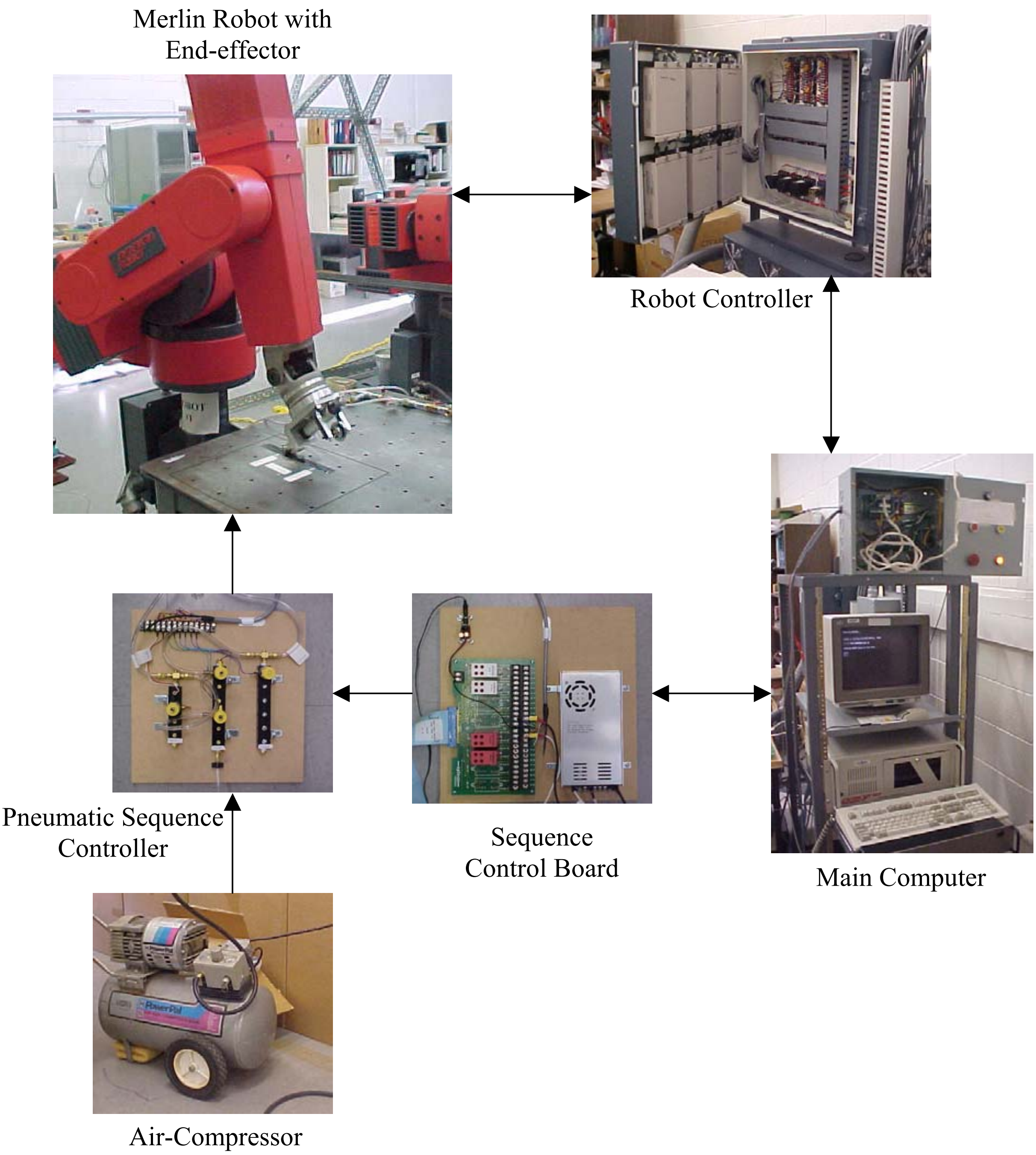

Figure 30. Compaction System Diagram

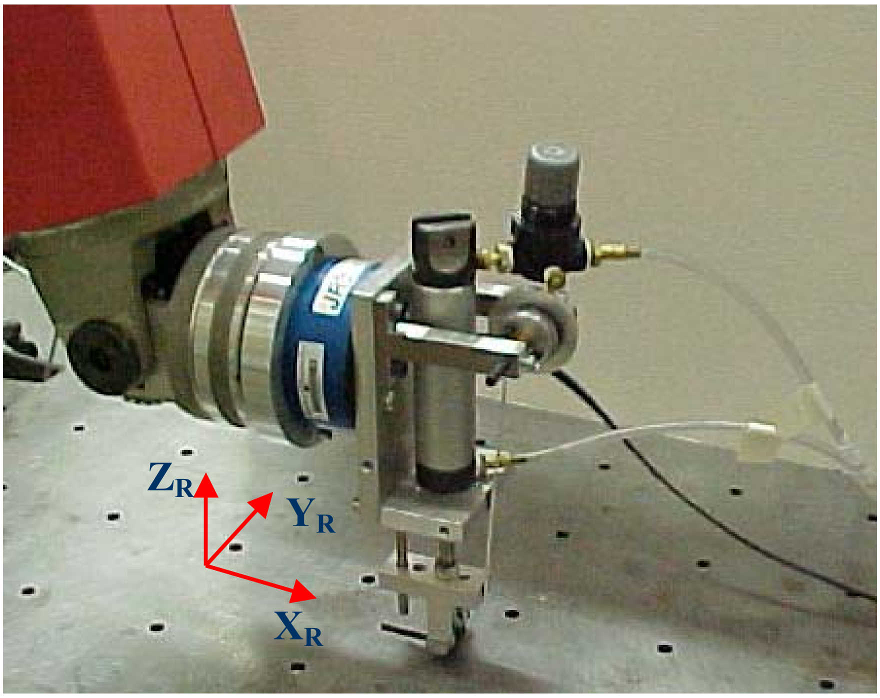

Figure 31. Tape Laying Process with a Robotic Compaction System and JR-3 Force Sensor

5.2 Static Compaction Force for Vertical Motion of a Pneumatic Mechanism

Since non-consistent compaction force was identified by the tactile sensor, a pneumatic mechanism with an air-cylinder was investigated for its possible variations that may affect the compaction force in a consolidation process. The Merlin robot oriented the pneumatic mechanism normal to the worktable shown in Figure 32, where the starting location was expressed in terms of

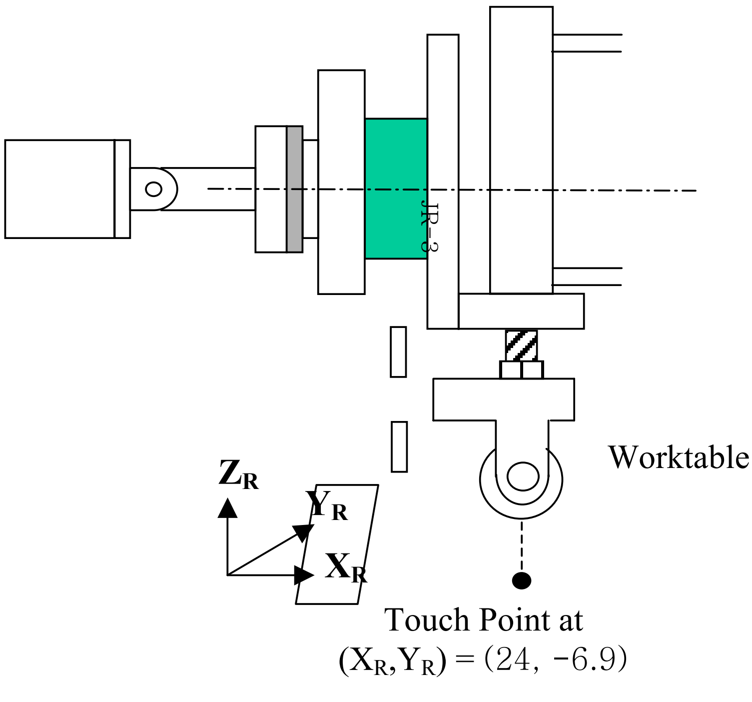

Figure 32. Schematic of Static Compaction Force Measurement with a JR-3 Force/Torque Sensor aligned normal to the Worktable (unit: inch)

global robotic coordinates, X_R,Y_R, and Z_R. The compaction mechanism was positioned at location (X_R,Y_R,Z_R) = (24", -11.9",-10.26"), with the roller lifted one inch from the surface of the worktable. At the same time, the pneumatic sequence controller was commanded to pull the piston inside the cylinder. Next, the compaction mechanism was driven straight down by the air-cylinder until the roller touched the worktable. This position was maintained for approximately six seconds while the compaction force reached a steady state condition. Upon reaching the steady state, the robot was commanded to move downward 0.1 inches with a velocity of 0.5 inch/sec and then hold this new position for four seconds. Next, two more iterations of downward movement (0.1 inches) were executed with each accompanied by a four second pause. At this point the robot was commanded to raise the compaction mechanism in a stepwise fashion similar to the previous steps. The robot moved the mechanism upward 0.1 inches and paused at the new position for four seconds. This was repeated three times restoring the compaction mechanism to the original position. Throughout the entire process of lowering and raising the compaction mechanism, the air-pressure inside the air-cylinder was maintained constant by the use of a relief value.

Figure 33 shows the compaction force as measured by the JR3 force/torque sensor at seven points through the compaction process. This figure shows two plots of the measured hysteresis with an air-pressure of 18 psi at the bottom, and two plots with an air-pressure of 20 psi at the top. The maximum compaction force differences were 2.035 lb for a 20 psi air-pressure and 1.024 lb for an 18 psi air-pressure. These force differences were 7.3% and 4.7% deviations for 28 lbs and 20 lbs of compaction force respectively. Even though a relief valve was installed between the air-cylinder and air compressor, hysteresis was still observed. In order to avoid this hysteresis, the compaction mechanism needed additional controls.

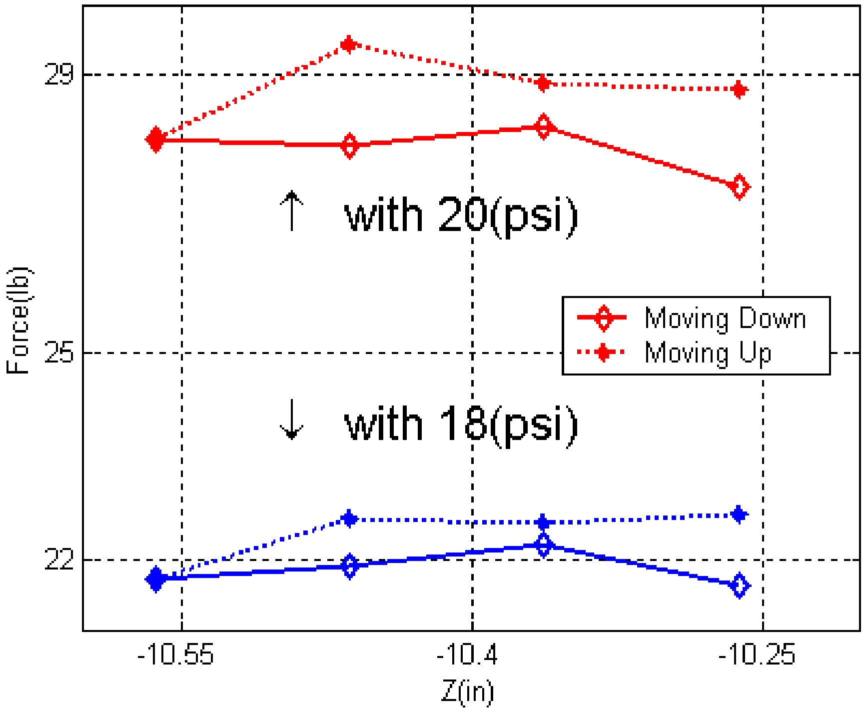

Figure 33. Non-linear Compaction Force along Z-direction for Two Different Air-pressures inside the Air-cylinder

To quantify the possible effect of hysteresis by the pneumatic compaction mechanism on the quality of a composite, the strength variation was theoretically calculated. According to Hulcher, et al. [54], the compaction load could affect the average strength of the composite by 13.4 kN/m per 1 kN change for the same test conditions with a particular thermoplastic. The compaction force change from the hysteresis effect is 9.05 N in SI unit, and this amount can affect the average strength of the thermoplastic composite by 0.121 kN/m. Considering the average strength was 4.89 kN/m for 1.11 kN compaction load, the possible average strength change of the thermoplastic composite resulting from hysteresis is 2.47 %. Since this force variation for the 0.3 inches of air-cylinder compression can change the strength of the composite parts theoretically, the hysteresis that may appear in conventional pneumatic compaction mechanisms should be eliminated for a consistent compaction force.

5.3 Compaction Force for Lateral Motion with Alternative Mechanisms

The compaction force profile with a pneumatic compaction mechanism driven by the Merlin robot is shown below in Figure 34. A roller end-effector in the mechanism was used to apply a compaction force. The robot moved the pneumatic compaction mechanism to (X_R,Y_R,Z_R) = (24", -11.9",-10.26") by a pneumatics sequence controller and then applied a downward compaction force in a

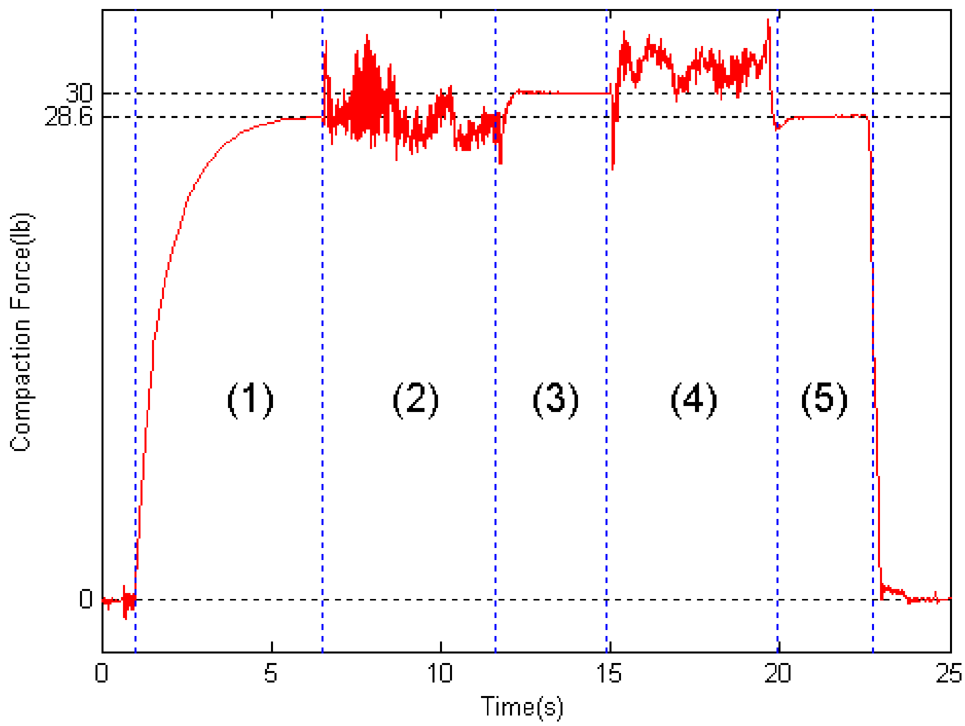

Figure 34. Dynamic Compaction Force Profile with a Pneumatic Compaction Mechanism at 20 psi of air-pressure while the Roller End-effector Moves Linearly with a 1 in/sec Speed on the Worktable

direction normal to the worktable. Thus, the roller end-effector installed at the end of the piston rod touched the start point (X_R,Y_R) = (24", -11.9") on the worktable, and subsequently the compaction force reached steady state (F_{start}) during zone (1). Upon reaching the steady state, the compaction mechanism was moved linearly on the worktable by the robot with a constant speed of 1 inch/sec and stopped at the end point (X_R,Y_R) = (29", -11.9") after 5 seconds of rolling. This time interval is represented by zone (2). For the next three seconds, zone 3, the compaction mechanism remained stationary at the new position with force F_{end}. Then during zone (4) the robot was commanded to move back along the same linear track with a constant speed of 1 inch/sec and stop at the original starting position, the restart point. At this position, the pneumatic mechanism was paused for 3 seconds with a static compaction force ($F_{restart}$). This interval is represented by zone (5). Throughout the entire linear motion process, air-pressure inside the air-cylinder was held constant at 22 psi using a relief valve and an air-pressure regulator.

5.3.1 Alternative Compaction Mechanisms

The major functions of a pneumatic compaction mechanism in the compaction process are to absorb impact when the compaction mechanism touches a structure surface and to regulate external disturbances, for instance, varying surface shape of a structure, start/end tape-laying, and machine vibration. The shock absorbers in a vehicle illustrate a concept similar to the pneumatic compaction mechanism. A vehicle uses a coil spring at each wheel with a damper that effectively absorbs an external impact and reduces vibrations. Thus, alternative compaction mechanisms comprising a spring with an air-cylinder were suggested and tested.

Three compaction techniques using a spring, a pneumatic, and a combined spring/pneumatic, were tested under similar conditions to compare the force profiles. The results of these tests are plotted in Figure 35 and quantitatively compared in Table 19. The spring had a spring constant of 26.05 lb/in. For the combined mechanism, the spring had a parallel connection with the air-cylinder.

From a control point of view [68], a spring, an air-cylinder, and the combination can be thought of as a proportional (P) controller, a derivative (D) controller, and a proportional/derivative (PD) controller respectively. However, these are simple open-loop controllers, such that feedback is not available for systematic compaction force control. Furthermore, the three mechanisms were independent each other and were experimentally tuned in order to make their static forces as close as possible: an air-pressure of 22 psi for the pneumatic mechanism, a spring deflection of 1.17 inches for the spring mechanism, and an air-pressure of 18 psi with a 0.28 inches of spring deflection for the combined mechanism. These three configurations were used during both the static and dynamic components of the compaction processes.

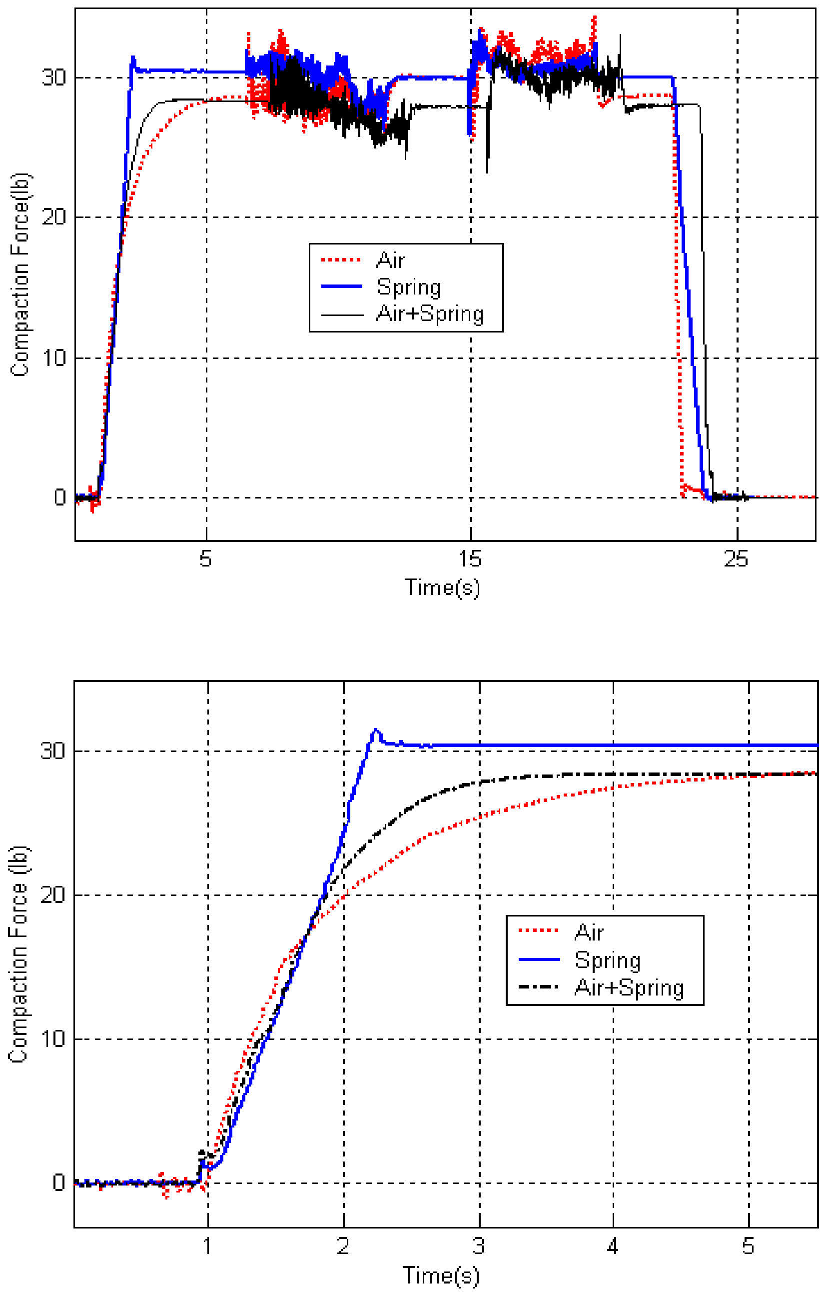

Figure 35. Compaction Force Histories with an Air-cylinder, a Spring, and Combined Mechanism (Top); Dynamic and Steady Compaction Force Histories with Three Different Compaction Mechanisms (Bottom)

Table 19. Comparison of Mechanisms : Quantitative Results from Figure 35

Quantities		Compaction Mechanisms		
		Air cylinder	**Spring**	**Spring and Air cylinder**
Static Compaction Fore (lb)	**Start Point**	28.57	30.39	28.34
	End Point	30.03	29.93	27.90
	Restart Point	28.66	29.98	28.03
	Force Difference	$\lvert F_{end}-F_{start}\rvert = 1.46$ $\lvert F_{end}-F_{restart}\rvert = 1.37$ $\lvert F_{restart}-F_{start}\rvert = 0.09$	$\lvert F_{end}-F_{start}\rvert = 0.46$ $\lvert F_{end}-F_{restart}\rvert = 0.05$ $\lvert F_{restart}-F_{start}\rvert = 0.41$	$\lvert F_{end}-F_{start}\rvert = 0.44$ $\lvert F_{end}-F_{restart}\rvert = 0.13$ $\lvert F_{restart}-F_{start}\rvert = 0.31$
Steady Dynamic	**Overshoot (lb)**	0	1.09	0
	Rise Time (sec)	5.27	1.26	2.35
	5% Settling Time (sec)	2.77	1.21	1.75
Unsteady Dynamic	**Peak-to-Peak (lb)**	7.28	4.94	6.63
Others		Air-pressure in the air-cylinder was 22 psi.	Deflection of the spring was 1.17.”	Air-pressure in the air-cylinder was 18 psi and Spring deflection was 0.28.”

* Air-pressures in the table were controlled by the air-pressure regulator and the relief valve.

5.3.2 Static Compaction Force Analysis

Static compaction forces were measured for lateral motion with each compaction system along the X_R-axis of the global robotic coordinates. The three points for these force measurements were the start point, the end point, and the restart point. Ideally, the static forces for each mechanism at all points should be the same. However, even when measurements were taken at the same point on the worktable, the compaction force again showed a non-linear characteristic, hysteresis. For example, with the pneumatic mechanism, the compaction force was measured at 28.57 lbs at the start point, 30.03 lbs at the end point, and 28.66 lbs at the restart point. Even though the first and last measuring points were the same position, 1.46 lbs of hysteresis was measured. This quantity is 5.1% of 28.57 lbs, and thus might adversely affect the quality of the composite in a consolidation process. The compaction method with the combined mechanism had the least hysteresis. As a result, the combined mechanism could be useful for providing a consistent static compaction force during a consolidation process.

5.3.3 Dynamic Steady Compaction Force Analysis

This section describes zone (1) in Figure 34. This interval represents the dynamic steady force, the part of the compaction force profile where the pneumatically induced compaction force reaches a steady state. One important characteristic of the dynamic steady force is the rise time, the time need to reach a steady state condition. This time may directly affect may directly affect the manufacturing speed of a composite towpreg with the compaction mechanism in fiber placement.

The compaction force profile with the air-cylinder had a long rise time and settling time but did not exhibit overshoot. The force profile with the spring mechanism showed a short rise time and settling time but also a high overshoot of 1.09 lbs. The combined compaction mechanism, however, exhibited good overall performance with no overshoot and a reasonably fast rise time and settling time when compared to the other compaction techniques.

5.3.4 Dynamic Unsteady Compaction Force Analysis

In Figure 34, zones (2) and (4) show a graph of the dynamic unsteady force. As illustrated by the graph in these zones, the dynamic and unsteady compaction force fluctuated significantly while the robot was moving the compaction mechanism. Such vibrations can potentially affect quality during fiber placement. According to Moon, et al. [58], one possible reason for tow boundary misalignment could be the vibration of the fiber placement head during the fiber placement process. Hence, the dynamic force profile will be investigated in detail.

The compaction force profile while the robot drives a pneumatic mechanism is shown in Figure 36. It is evident that the compaction force fluctuated significantly at (2) and (4) where the compaction force was dynamic and unsteady. The peak-to-peak compaction force was measured as 7.3 lbs, a signification amount given the overall compaction pressure of 28.57 lbs. Since the force variation was found to have a near normal distribution, it is inferred that there was no non-linear phenomena, such as roller wobbling or slipping, in the unsteady compaction profile.

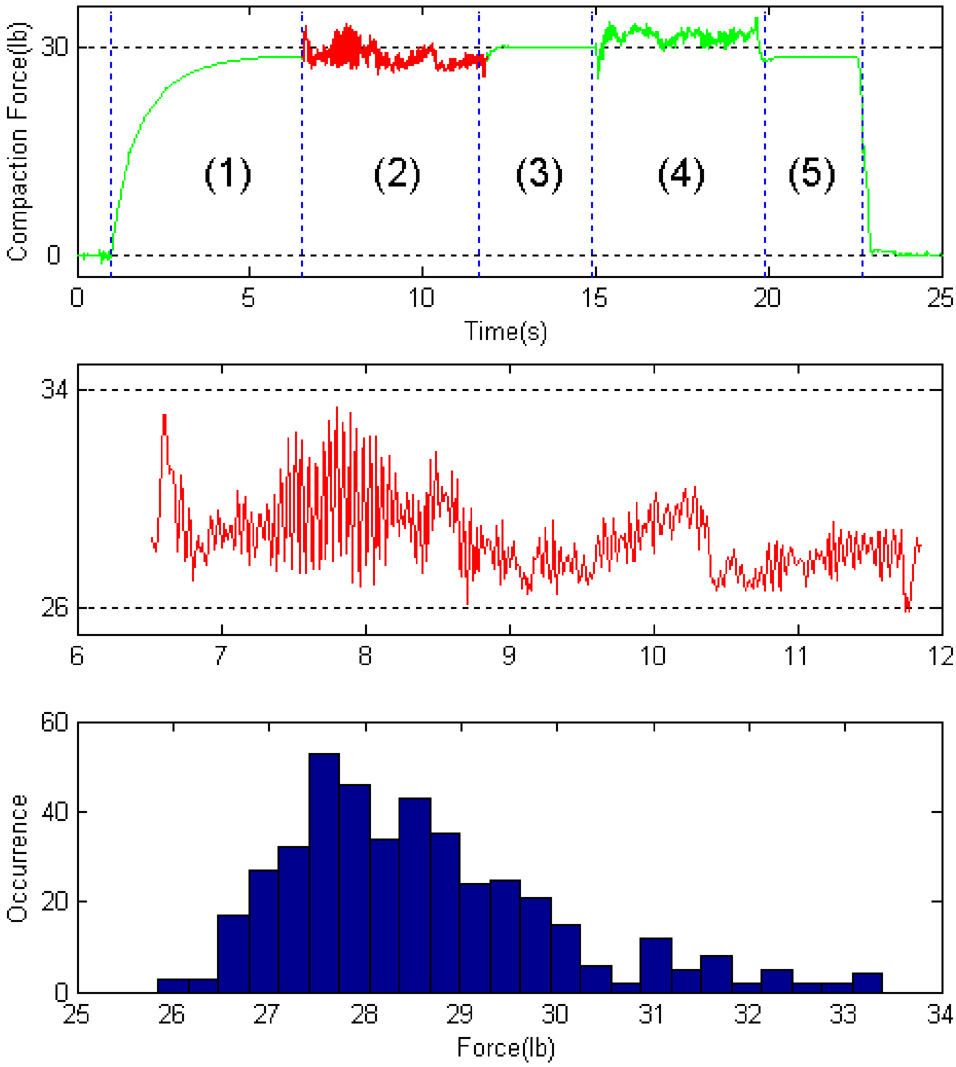

Figure 36. Compaction Force Profile with an Air-cylinder (top); Details of Unsteady Dynamic Force at (2) (middle); Distribution of the Dynamic Compaction Force Data in Section (2) (bottom)

In order to determine the cause of the dynamic unsteady force, the three compaction mechanism force profiles were analyzed using a Fast Fourier Transform (FFT) with a low pass filter to visualize the dynamic unsteady force in two-dimensions. Measurements made from the tactile force/pressure sensor shown in Figure 1 indicated that the frequencies of the unsteady compaction force on the sensor were relatively low. Hence, a low pass filter with a cut-off point set at 10 Hz was used to filter the high frequency vibrations before FFT analysis in Figure 37. This filtered profile was then analyzed through a Fast Fourier Transformation (FFT) technique.

The filtered compaction force profiles with different compaction mechanisms are shown in Figure 38, and FFT analysis results in Figure 39. The FFT results for three compaction mechanisms are very similar. These results lead to the conclusion that the dynamic unsteady force is not significantly affected by the compaction mechanism.

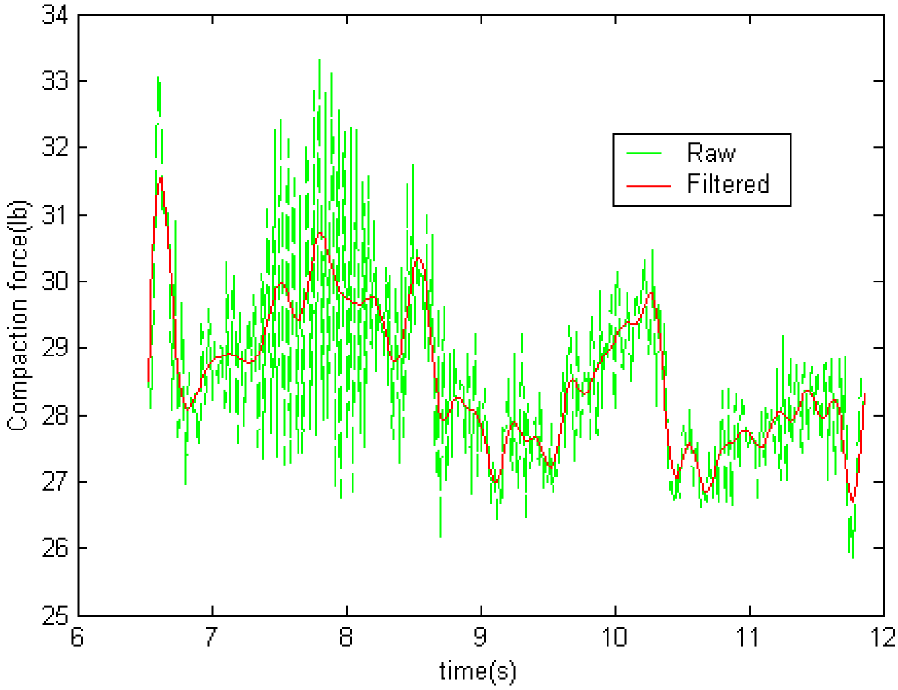

Figure 37. Filtered Dynamic Unsteady Compaction Force Profile through the Low Pass Filter with 10 Hz Cutoff Frequency

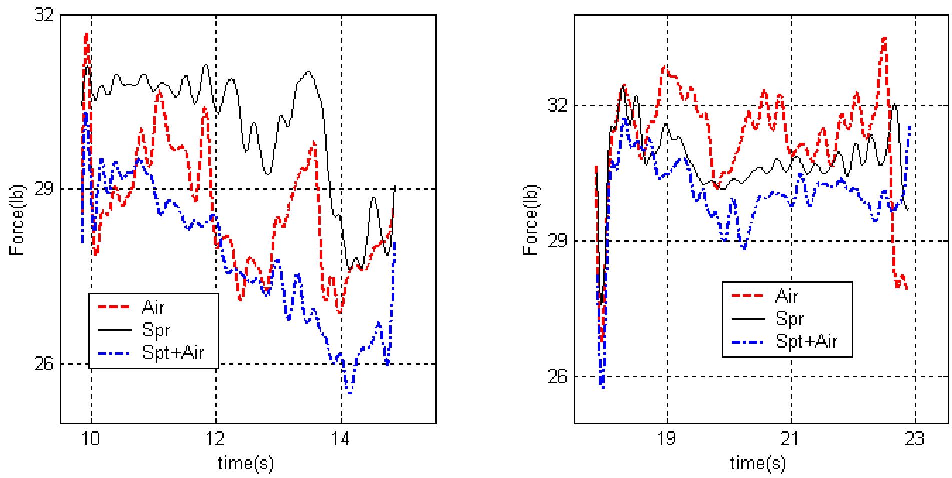

Figure 38. Low-pass Filtered Dynamic Unsteady Compaction Force Profiles with an Air-cylinder, a Spring, and a Combined; Positive X_R-directional Motion (Left) and Negative XR-directional Motion (Right)

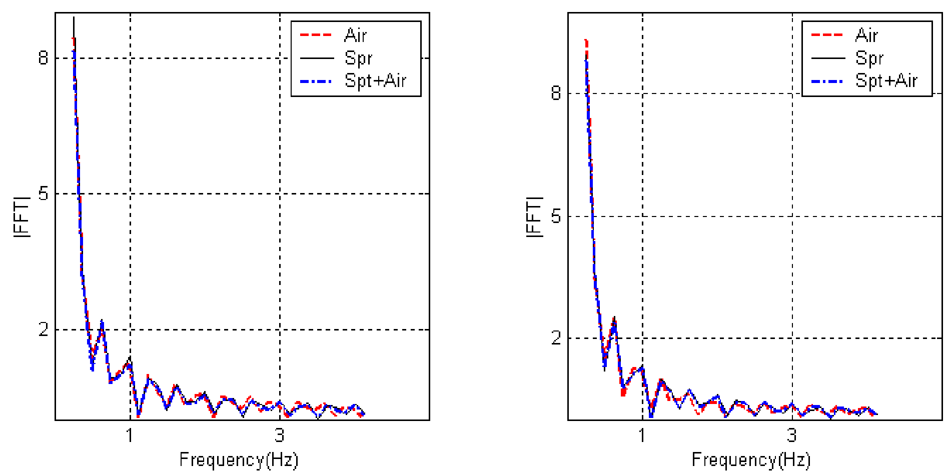

Figure 39. FFT of the Low-pass Filtered Compaction Forces; Positive X_R-directional Motion (Left) and Negative XR-directional Motion (Right)

5.3.5 Effect of a Robotic Compliance

Since the compaction mechanisms do not change the dynamic unsteady behavior, a locked mechanism functioning as a rigid body, was tested and compared with two other compaction techniques to find the main cause of the dynamic unsteady compaction force.

Three types of tests were done. The first test was done with a pneumatic mechanism, the second with a spring mechanism, and the third with a locked mechanism (rigid mechanism). The test results are plotted in Figure 40. Figure 41 shows the same data filtered through a low-pass filter, and Figure 42 shows the FFT analysis results.

The FFT results of the three end-effectors were again very similar. Therefore, it appeared that the variation exhibited in the dynamic unsteady force was a characteristic of the robot and not the mechanisms. As the robot drives the mechanism to a desired position, robotic compliances are the most likely source of the disturbance. This characteristic of robotic compliance should be further investigated to enhance the consistency of the compaction force.

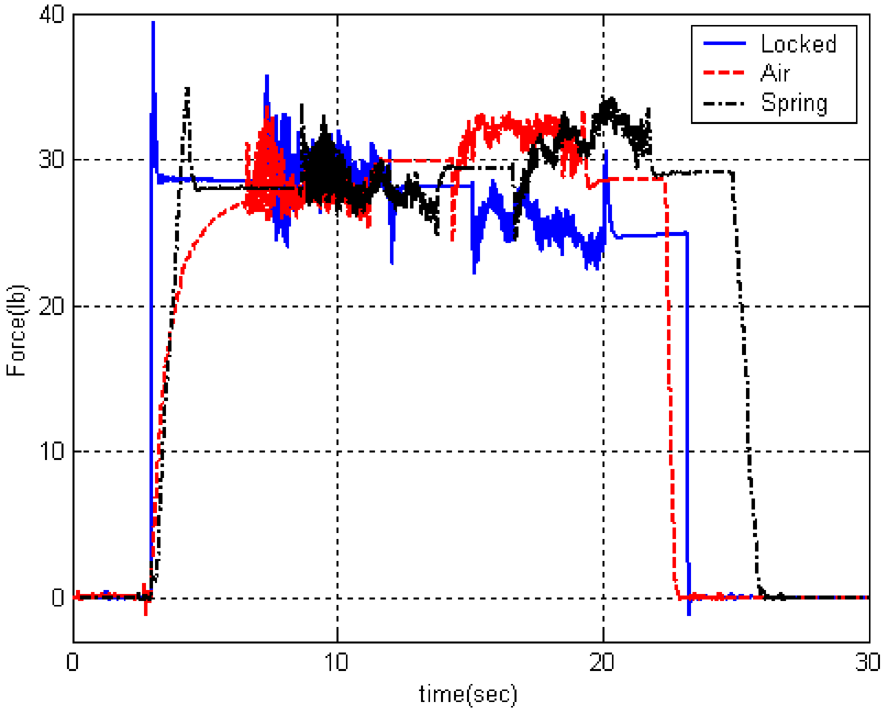

Figure 40. Unsteady Dynamic Compaction Force Profiles with a Locked, with an Air-cylinder, and with a Spring Mechanisms

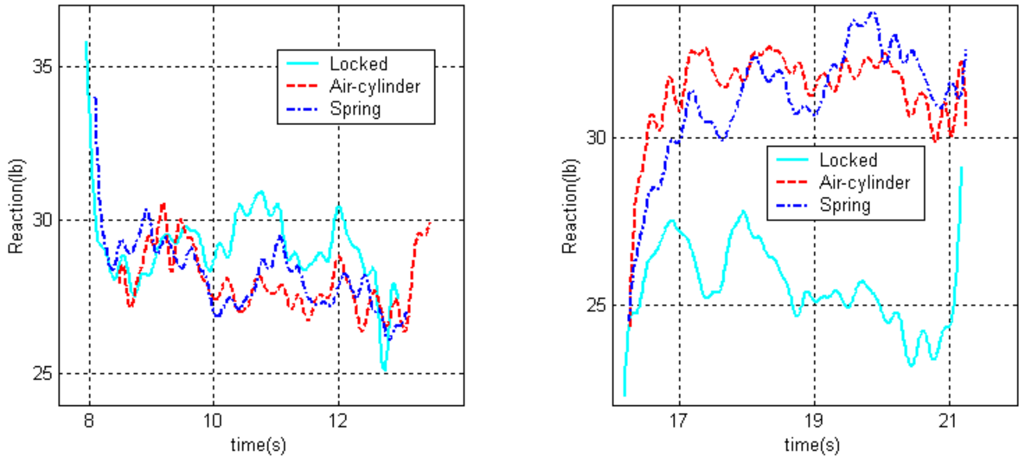

Figure 41. Low-pass Filtered Compaction Force Profiles with a Locked, with an Air-cylinder, and with a Spring End-effector; Positive X_R-directional Motion (Left) and Negative X_R-directional Motion (Right)

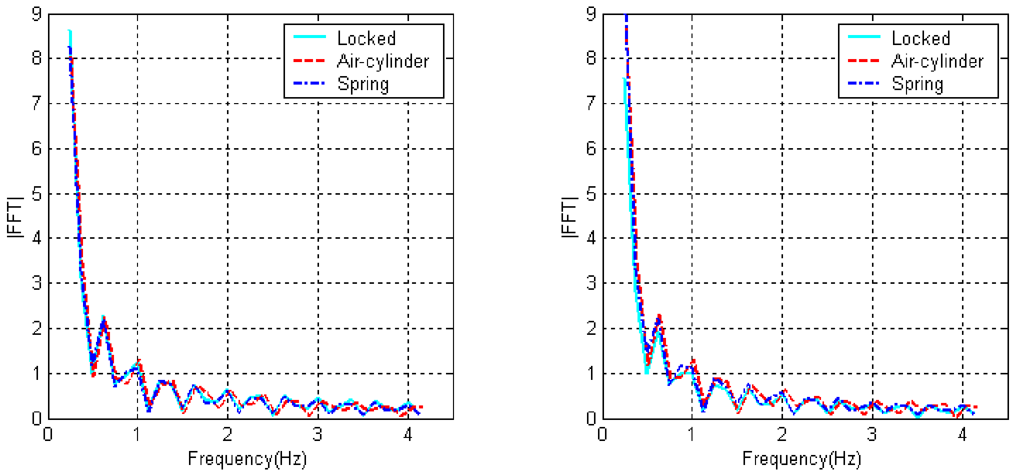

Figure 42. FFT of the Low-pass Filtered Compaction Forces; Positive X_R-directional Motion (Left) and Negative XR-directional Motion (Right)

6 Concluding Remarks

Automated fiber placement, as one of the advanced composite manufacturing processes, provides a solution to the cost problem associated with expensive hand lay-up based composites processes. Even though complex chemical and physical sub-processes are involved in the process, many researchers in the field found major process parameters, such as pre-heating temperature, nip-point temperature, compaction force, manufacturing speed, towpreg tension, and towpreg viscosity [39,40,45,54]. Each parameter could be characterized by a combination of the fiber placement machine components and their dynamic properties.

From the function block diagram (FBD) development of the conceptual advanced fiber placement process, it was found that heating and compressing sub-processes of a towpreg are important factors that can affect two major parameters, nip-point temperature and compaction force, producing better composite structure quality. Hence, the towpreg heating process with new heating alternatives, liquid and rigid contact, was studied and compared with the widely used gas heating technique. Additionally, the accuracy of the compaction force during the compaction process was identified while a robotic machine with a pneumatic tool moved on a rigid worktable.

6.1 Summary

6.1.1 Heat Transfer Modeling of a Towpreg

A current and widely used heating method uses a hot gas heating because of its low cost and flexible installation [61~65]. Alternative heat sources, liquid and rigid contact, were suggested and compared with the gas heat source with respect to feasibility of use in advanced fiber placement processing. First, composite towpreg modeling was conducted to incorporate an external heat source application to a composite towpreg. Since the towpreg composite, Fiberite 977-2 Toughened Epoxy Neat Resin thermoset, is assumed to be very thin and linear, a one-dimensional model along the thickness with uniform material properties was employed for the modeling. Subsequently, a heat transfer model between each heat source and the composite model was used to gauge composite manufacturing speed and heat source energy efficiency.

The results showed that a rigid contact heat source is an outstanding candidate heat source for its high speed. A liquid heat source and a gas heat source, in this order, follow with manufacturability. For an effective heating area 1×1 cm^2 on the composite towpreg, which has 0.3 mm thickness and 0.635 cm width, the rigid contact heating is at least 18 times faster than the hot air heating with an average convective heat transfer coefficient of 260 $W/m^2/°C$. With respect to energy efficiency, a rigid heat source is again found to be the outstanding candidate heat source. Rigid heating is at least 13 times better than gas heating in this respect.

Additionally, the rigid contact heating has a low sensitivity for heating time tolerance that the sensitivity of the gas heating: ±2.67°C for ±0.01 seconds of heating time tolerance for the rigid contact and ±13.4°C for the same tolerance with the gas heating. The temperature of the towpreg does not exceed the heat source temperature for an excessive heating time; thus, it is a very safe heating method. The ability of uniform heating over the effective heating area is a good advantage of the rigid contact heating as well.

However, each heat source has other advantages and disadvantages. Gas heat source has been used for its installation flexibility and low-cost facility equipment. Research in this approach has been done for many years and collected data are available in [39,40,44]. On the other hand, manufacturing speed is very slow and energy efficiency is very low. A liquid heat source carries new critical limitations, such as non-volatility for a wide range of temperatures, and needs to be chemically non-reactive with the composite. Also, liquid recycling cost and environmental effects should be seriously considered even though its manufacturing speed is faster than gas. A rigid contact heat source has excellent advantages in manufacturing speed and energy efficiency. However, it requires a heating filament controller and the heated composite towpreg must not stick on the rigid heat source.

For these pros and cons, liquid and rigid heating methods are very efficient ways of composite manufacturing as compared with the widely used hot gas heating process from the research results. The rigid contact heating technique is particularly promising. Thus, this heating source needs to be further developed to a realistic heating roller for automated fiber placement.

6.1.2 Modeling of a Rigid Heating Roller in contact with a Towpreg

Development of a rigid heat source involves a conceptual rigid roller design to gauge the controllability of the roller surface temperature and the towpreg temperature. A linear two-dimensional roller model was developed with respect to the radial and angular directions of the roller cross-section for static and quasi-static heating processes. Finite element models of a rigid heating roller and a composite towpreg were employed for conduction heat transfer analysis between the roller and the composite towpreg. The rigid heating roller was made of hollow transparent Pyrex material with black Teflon coating outside and a heating filament inside the roller.

Static heating of a roller was simulated without towpreg contact for 7 seconds. A 45.68°C of overshoot and a rise time of 0.32 seconds were identified with an ON/OFF controller, and a 3.31°C overshoot and 0.42second rise time were found using a P controller. Quasi-static heating of a roller in contact with a towpreg is simulated with a 120 degree towpreg contact angle for 6 seconds with a PD controller. The final temperature of a composite towpreg was controlled at the minimum temperature of 190.7°C and within a 2.51°C fluctuating band with an outer radius (Ro) of 2.51cm and a radial thickness of 0.155cm. From these simulation results, a rigid heating roller is expected to have good temperature controllability, and thus, the heat transfer from the rigid tool to the composite towpreg is also well controllable. Therefore, a rigid contact heat roller with a PD controller is a very promising heat source for advanced fiber placement.

6.1.3 Compaction Force Analysis

One of the main process parameters, compaction force, was investigated in detail to find the possible effects on the process. First, the pneumatic compaction mechanism without an accurate control had a hysteresis. Second, the combined mechanism of an air-cylinder and a spring is recommended to get the best result of a steady compaction force. Third, the compaction force was fluctuating while the pneumatic mechanism moves on the worktable by the robot. The main reason for the dynamic unsteady compaction force was the robot. To improve the quality of the composite through the fiber placement process, robotic compliance needs be investigated.

6.1.4 Conclusion

The goal of this dissertation is to develop efficient and more controllable sub-processes for automated fiber placement. New heat sources were suggested in an attempt to find a better controllable heat transfer model that could provide a reliable and consistent heating process for the fiber placement process. As a result, rigid contact heating is a promising alternative for its manufacturing speed and energy efficiency. In the heat transfer modeling, a thermoset composite material was targeted and analyzed. However, the approach used could be useful for the analyses of other thin composite materials. For example, with the replacement of thermal material properties, boundary conditions, and material specifications, the same governing equations could give response time, and thus, manufacturing speeds for different heat sources. Furthermore, the conceptual heating roller model could give an efficient design and analysis tool in the contact heating process of many kinds of composites. In addition, compaction force that has been neglected in the existing composite fabrication processes was discussed to enhance the final parts quality through the consistent consolidation process. It is hoped that this heat transfer and consolidation modeling for composite fiber tow heating with a new rigid contact heating tool could contribute to composite fabrication fields.

6.2 Future Work

As future work of the research in this dissertation, following activities are recommended to develop further the rigid contact heating.

1. Simulations with a low emissivity reflector to concentrate the lamp energy
2. Designing a rigid contact heating roller and system making test articles and their subsequent validation with respect to the test protocol
3. Development of the heat transfer model using the test results
4. Apply the Taguchi method to optimize parameters of the rigid heating roller
5. Development of an analytical compaction model to control the mechanism connected to the robot
6. Simulation with the same rigid heating tool but with varying speed

References

[1] Loos, A. C., Sturges, R. H., Viehland D., "Non-autoclave Processing and Manufacturing of Large Reusable Aerospace Structures," Research Proposal for NCAM Louisiana Partnership University of New Orleans Research Technology Foundation, 2001.

[2] Coffenberry, B. S., Hauber, D. E., Cirino, M., "Low Cost Alternative: In-Situ Consolidated Thermoplastic Composite Structures," 38th International SAMPE Symposium, pp. 1640 – 1650, 1993.

[3] Schwartz, M. M., "Composite Materials," Vol I and II, prentice Hall, NJ, 1997.

[4] Fowler, Theodore C., "Value Analysis in Design," Van Nostrand Reinhold, 1990.

[5] Sturges, R., O′Shaughnessy, K., Reed, R., "A systematic Approach to Conceptual Design," Concurrent Engineering: Research and Application 1, 93-105, 1993.

[6] Sturges, R., O′Shaughnessy, K., Kilani, M., "Computational model for conceptual design based on extended function logic," Artificial Intelligence for Engineering Design, Analysis and Manufacturing(1996), 10, 255 – 274.

[7] Colton, J., Leach, D., "Processing Parameters for Filament Winding Thick-Section PEEK/Carbon Fiber Composites," Polymer Composites, Vol. 13, No. 6, pp. 427- 434, 1992.

[8] Grove, S. M. "Thermal Modeling of Tape Laying with Continuous Carbon Fiber-Reinforced Thermoplastic," Composites, Vol. 19. No. 2. pp. 367-375, 1988.

[9] Beyeler, E. P. and Güçeri, S. I., "Thermal Analysis of Laser-Assisted Thermoplastic-Matrix Composite Tape Consolidation," ASME Journal of Heat Transfer, 110, pp. 424-430, 1988.

[10] Ghasemi Nejhad, M. N., Cope, R. D., Güçeri, S. I., "Thermal Analysis of In-Situ Thermoplastic-Matrix Composite Filament Winding," ASME Journal of Heat Transfer, 113, pp. 304-313, 1991.

[11] Bogetti, T. A. and Gillespie, J. W., "Process-Induced Stress and Deformation in Thick-Section Thermosetting Composite Laminates," 21st International SAMPE Technical conference, Sep. 25-28, pp. 947-959, 1989.

[12] Bryant, E. and Klosterman, D., Flach, L., Chartoff, R., "Development and Verification of a Thermal Model For Curved-Layer Laminated Object Manufacturing (LOM)," 44th International SAMPE Symposium & Exhibition, Long Beach, CA, May 1999.

[13] Lee, W. I. and Springer, G. S., “A Model for the Manufacturing Process of Thermoplastic Matrix Composites,” Journal of Composite Materials, Vol. 26, No. 16, pp. 2348-2410, 1987.
[14] Sun, W. C., Mantell, S. C., Stelson, K. A., “Modeling and Control of the In-Situ Thermoplastic Composite Tape-Laying Process,” Journal of Dynamic Systems, Measurement, and Control, Vol. 120, pp. 507-515, 1998.
[15] Carpentrer, C. E. and Colton, J. S., “On-Line Consolidation Mechanism in Thermoplastic Filament Winding (Tape-Laying),” 38th International SAMPE Symposium, pp. 205-216, 1993.
[16] Pitchumani, R., Don, R. C., Gillespie, J. W., Ranganathan, S., “Analysis of On-Line Consolidation during Thermoplastic Tow-Placement Process,” Thermal Processing of Materials, Published by ASME, Heat Transfer Division, Vol. 289, pp. 223-239, New York, NY, 1994.
[17] Heider, D., Foulk, R. M., Gillespie, J. W., Jr, “Adaptive Temperature Control for the Thermoplastic Tow-Placement Process,” 43rd International SAMPE Symposium, pp. 214 – 224, 1998.
[18] Bogetti, T. and Gillespie, J., Jr., “Two-Dimensional Cure Simulation of Thick Thermosetting Composites,” Journal of Composite Materials, Vol. 25, pp. 239 – 269, 1991.
[19] Ghasemi Nejhad, M. N., Cope, R. D., Güçeri, S, I., “Thermal Analysis of in-situ Thermoplastic Composite Tape Laying,” Journal of Thermoplastic Composite Materials, Vol. 4, pp. 20-45, 1991.
[20] Wells, G. M. and McAnulty, K. F., “Computer Aided Winding Using Non-Geodesic Trajectories,” Proceedings, 6th International Conference on Composite Materials, 2nd European Conference on Composite Materials, 1:1.161-1.173, 1987.
[21] Barth, J. R., “Fabrication of Complex Composite Structures using Advanced Fiber Placement Technology,” 35th International SAMPE Symposium, pp.710–720, 1990.
[22] Hauber, D. E., Hardtmann, D. J., Bubeck, K. B., “Recent Advances in Thermoplastic Composite Fabrication using ROWS,” 35th International SAMPE Symposium, pp. 767-771, 1990.
[23] Enders, M. L., Hopkins, P. C., “Developments in the Fiber Placement Process,” 36th International SAMPE Symposium, pp. 778-790, 1991.
[24] Burgess, J. B., Wilenski, M. S., Belvin, H. L., Cano, R. J., Johnson, N. J., “Development of a Cure-On-The-Fly Automated Tape Placement Machine for Electron Beam Curable Prepregs,” 46th International SAMPE Symposium, pp. 2024-2036, 2001.

[25] Beloy, J. M. and Mantell, S. C., "Investigation of Tape-Laying Process Parameters," Journal of Materials Processing and Manufacturing Science, Vol. 4, pp. 279-298,1996.
[26] Calhoun, D. R., "Modeling of the On-line Consolidation Processing of Thermoplastic Filament Winding," SME Fabricating Composites, Arlington, TX, 1990.
[27] Beyeler, E. P. and Güçeri, S. I., "Thermal Analysis of Laser-Assisted Thermoplastic-Matrix Composite Tape Consolidation," ASME Journal of Heat Transfer, 110:424-430, 1988.
[28] Beyeler, E. P., Phillips, W. A., Güçeri, S. I., "Experimental Investigation of Laser Assisted Thermoplastic Tape Consolidation," Journal of Thermoplastic Composite Materials, Vol. 1, 1989.
[29] Güçeri, S. I., "On-Line (In-Situ) Consolidation of Thermoplastic Composites – a Review," The Eighth Thermoplastic Matrix Composites Review, University of Delaware, 1991.
[30] Irwin, R. G. and Güçeri, S. I., "Recent Advances in Laser Heated On-line Consolidation of Thermoplastic Composites," Heat Transfer Effects in Materials Processing ASME HTD-Vol. 233, 53-60, 1992.
[31] Mazumdar, S. K. and Hoa, S. V., "Experimental Determination of Process Parameters for Laser Assisted Processing of PEEK/Carbon Thermoplastic Composites," 38th International SAMPE Symposium, pp. 189-203, 1993.
[32] Sharp, R. S, Holmes, C. Woodall, "Material Selection/Fabrication Issues for Thermoplastic Fiber Placement," Journal of Thermoplastic Composite Materials, 8:2-14, 1995.
[33] Werdermann, C., Friedrich, K., Cirino, M., Pipes, R. B., "Design and Fabrication of an On-Line Consolidation Facility for Thermoplastic Composites," Journal of Thermoplastic Composite Materials, 2:293-306, 1989.
[34] Haupert, F., Chen, C., Friedrich, K., "Manufacturing of Thermoplastic Composite Parts by Combined Filament Winding and Injection Molding," Proceeding ICCM 10, Canada, Aug. 1995.
[35] Endres, M., "Developments in Thermoplastic Filament Winding," 22nd International SAMPE Technical Conference, Boston, MA, 1990.
[36] Calhoun, D. R., "Modeling the On-line Consolidation Processing of Thermoplastic Filament Winding," SME Fabricating Composites, Arlington, TX, 1990.
[37] Steiner, K.V., "Development of a Robotic Filament Winding Workstation for Complex Geometry," 35th International SAMPE Symposium, pp. 757-766, 1990.
[38] www.coastaltoner.com/copy_process_explanation.html (10 December 2003)

[39] Shih, Po-Jen and Loos, A., "On-Line Consolidation of Thermoplastic Composites," Dissertation, Center for Composite Materials and Structures, Feb. 19, 1997.
[40] Klasus D. Felderhoff, Karl V.Steiner, "A New Compact Robotic Head for Thermoplastic Fiber Placement," 38th int'l SAMPE Symposium, May 10-13, pp 138 – 151, 1993.
[41] Endres, M. L. and Hopkins, P. C., "Development in the fiber placement process," 36th int'l SAMPE Symposium, April 15-18, pp 778 – 790, 1991.
[42] Chen, M., Craig, K., and Domoto, G., "On control of distributed, non-steady state, thermal system: A comparison between simulation and experimentation," the 7th Mechatronics Forum International Conference, Sep 6-8, 2000.
[43] Chen, M., Craig, K., and Domoto, G., "Modeling of A Distributed, Non-Steady State, Thermal System For The Purpose of Control," Mechatronics 98, pp.211-216, Sep. 9-11, 1998.
[44] Steiner, K. V., "Development of a Robotic Filament Winding Workstation for Complex Geometries," 35th int'l SAMPE Symposium, April 2-5, pp 757 – 766, 1990.
[45] Hummler, J., Lee, S.K., Steiner, K.V., "Recent Advances in thermoplastic Robotic Filament Winding," 36th int'l SAMPE Symposium, April 15-18, pp 2142 – 2156, 1991.
[46] Martin, J., Langone, R., Pasanen, M., Mondo, J., "Cost-effective, automated equipment for advanced composite structure development and production," Automated Dynamics Corporation, 407 Front St., Schenectady, NY, 12305-1036. (September 2001)
[47] Martin, J., Langone, R., Pasanen, M., Mondo, J., "Advanced composite fiber placement: Process to application," Automated Dynamics Corporation, www.automateddynamics.com/advanced_composite.PDF (10 January 2004)
[48] Thomas, L., "Heat Transfer," Prentice Hall, Englewood Cliffs, NJ, 1992.
[49] Incropera and DeWitt, "Introduction to Heat Transfer," 3rd edition, New York, John Wiley & Sons, 1996.
[50] Shacklford, J., Alexander, W., "CRC Materials Science and Engineering Handbook," 3rd edition, CRC, 2001.
[51] Serpentine type II heat exchanger specification, Osram Sylvania Inc., www.thermalinc.com/electheaters/index.htm (10 November 2002)
[52] Farlow, S. J., "Partial Differential Equations for Scientists and Engineers," New York, John Wiley & Sons, 1982.
[53] http://www.mathworks.com/access/helpdesk/help/toolbox/pde/pde.shtml
[54] Hulcher, B., Banks, W. I. III, Pipes, R. B., Tiwari, S. N., Cano, R. J., Johnston, N. J., "Automated Fiber Placement of PEEK/IM7 Composites with Film

Interleaf Layers," 46th International SAMPE Symposium, May 6-10, 2001, pp. 1998-2012.
[55] Sensor Products Inc. 188 Route 10 E. Hanover, NJ 07936 USA, www.sensor.com (11 January 2003)
[56] JR3 Inc., www.jr3.com/index.html (20 November 2003)
[57] Software and Installation Manual for JR-3, JR3, Inc., 22 Harter Ave. Woodland, CA, 95776.
[58] Moon, R. S. and Johnson, C. C., Hale, R. D., "Nondestructive Evaluation and Mechanical Testing of Steered Fiber Composites", 47th international SAMPE Symposium, pp.1550 – 1563, May 12-16, 2002.
[59] Merlin System Operator's Guide, Version 3.0, American Robot Incorporation. (June 1985)
[60] http://www.americanrobot.com (10 November 2003)
[61] Colton, J. and Leach, D., "Processing Parameters for Filament Winding Thick-Section PEEK/Carbon Fiber Composites," Polymer Composites, 13(6), pp. 427-434, 1992.
[62] Cirono, M., Waston, T. P., Hauber, D. E., "Composite Structure Fabrication with In-Situ Consolidation of APC-2/AS4," 36th International SAMPE Symposium, pp. 2184-2196, 1991.
[63] Buijs, J.A.H.M. and Nederveen, P.J., "A Study of Consolidation in Filament Winding with Thermoplastic Prepregs," Journal of Thermoplastic Composite Materials, 5, pp. 276-286, 1992.
[64] Carpenter, C. E. and Colton, J. S. "On-Line Consolidation Mechanism in Thermoplastic Filament Winding (Tape-Laying)," 38th International SAMPE Symposium, pp. 205-216, 1993.
[65] Carpenter, C. E. and Colton, J. S. "On-Line Consolidation Mechanism in Thermoplastic Filament Winding," Polymer Composites, 15(1), pp. 55-63, 1993.
[66] www.compositesworld.com
[67] file:///C:/Documents%20and%20Settings/lee%20munki/Local%20Settings/Temporary%20Internet%20Files/Content.IE5/SHAJ8DIF/271,21,Benefits To Repair & Sustainability
[68] Franklin, Powell, and Emami-Naeini, "Feedback Control of Dynamic Systems," 3rd edition, Addison-Wesley, 1994.
[69] http://www.mathworks.com/access/helpdesk/help/toolbox/signal/signal.shtml (Jun 2003)
[70] http://www.clippard.com/downloads/general/pdf_documents/august_2003_full_catalog_by_catagory/cylinders/minimatic_brass_and_aluminum_cylinders.pdf (Oct 2003)
[71] www.wilkersoncorp.com/product/filter-regulator.html (Dec 2003)

[72] www.autospeed.com/cms/A_0670/printArticle.html (Dec 2003)

Appendix

A-1 Terminologies of the Automated Fiber Placement [3,66,67]

Advanced composite: High-performance or cost-performance material

Composite: A homogeneous material created by the synthetic assembly of two or more materials to obtain specific characteristics and properties

Consolidation: A processing step that compresses fiber and matrix to reduce voids and achieve a desired density

Debulk: The compacting or squeezing out of air and volatiles between plies or prepreg laminates under moderate heat and vacuum to insure seating on the tool, to prevent wrinkles, and to promote adhesion.

Fiber placement: Continuous process for fabricating composite shapes with complex contours and/or cutouts by means of a device that lays preimpregnated fibers (in tow form) onto a nonuniform mandrel or tool. Differs from filament winding in several ways: There is no limit on fiber angles; compaction takes place online via heat, pressure or both; and fibers can be added and dropped as necessary. The process produces more complex shapes and permits a faster putdown rate than filament winding.

Filament winding: A process for fabricating a composite structure in which continuous reinforcement (filament wire, yarn, tape, or other) impregnated with a matrix material either previously or during the winding are placed over a rotating removable form or mandrel in a prescribed way to meet certain stress conditions

Filaments: Individual glass fibers of indefinite length, usually as pulled from the stream of molten glass flowing through an orifice of the bushing

Geodesic: The shortest distance between two points on a surface

Layup: Process of placing layers of reinforcing material placed in position in the mold

Matrix: The dominating lattice structure of a given phase in a material; the essentially homogeneous resin or polymer material in which the fiber system of a composite is imbedded

Ply: The number of single yarns twisted together to form a plied yarn; one of the layers that make up a stack or laminate

Prepreg: Ready-to-mold material in sheet form, which may be cloth, mat, or paper impregnated with resin and stored for use

Processing window: Probability of good parts of composites

Tape: A composite ribbon consisting of continuous or discontinuous fibers aligned along the tape axis parallel to each other and bonded together by a continuous matrix phase

Tape laying: A fabrication process in which prepreg tape is laid side by side or over-lapped to form a structure

Thermoplastic: Capable of being repeatedly softened by an increase in temperature and hardened by a decrease in temperature; applicable to materials whose change upon heating is substantially physical rather than chemical and can be shaped by flow into articles by molding and extrusion

Thermoset: A plastic that changes into a substantially infusible and insoluble material when it is cured by application of heat or by chemical means

Tow: A large bundle of continuous filaments, generally 10000 or more, not twisted

Towpreg: A prepreg fabricated from tow which can be converted to woven and braided fabric

Vita

Munki Lee was born August 1968 in Taegu Korea. He received his Bachelor of Science in Mechanical Engineering from Pohang University of Science & Technologies in Korea, 1992. After he got his Bachelor's degree, he participated in an Unmanned Vehicle Dynamic System development project funded by Hyundai in Korea, 1992. After serving Korean Air-Force for 3 years as a Lieutenant, he joined KIA Motor Company as a research associate in Korea, 1997.

He got his Master of Science degree in Mechanical Engineering from Mississippi State University, Starkville, MS, 1999. Also, He graduated from Virginia Polytechnic Institute & State University in Mechanical Engineering with a Doctor of Philosophy, Blacksburg, VA, 2004.